PLOS PATHOGENS

RESEARCH ARTICLE

Bartonella effector protein C mediates actin stress fiber formation via recruitment of GEF-H1 to the plasma membrane

Simon Marlaire, Christoph Dehio*

Biozentrum, University of Basel, Basel, Switzerland

* christoph.dehio@unibas.ch

Citation: Marlaire S, Dehio C (2021) *Bartonella* effector protein C mediates actin stress fiber formation via recruitment of GEF-H1 to the plasma membrane. PLoS Pathog 17(1): e1008548. https://doi.org/10.1371/journal.ppat.1008548

Editor: Zhao-Qing Luo, Purdue University, UNITED STATES

Received: April 11, 2020

Accepted: October 9, 2020

Published: January 28, 2021

Data Availability Statement: All relevant data are within the manuscript and its Supporting Information files.

Funding: This work was supported by grant 31003A_173119 from the Swiss National Science Foundation (SNSF, www.snf.ch) to C.D. The funders had no role in study design, data collection and analysis, decision to publish, or preparation of the manuscript.

Competing interests: No

Abstract

Bartonellae are Gram-negative facultative-intracellular pathogens that use a type-IV-secretion system (T4SS) to translocate a cocktail of *Bartonella* effector proteins (Beps) into host cells to modulate diverse cellular functions. BepC was initially reported to act in concert with BepF in triggering major actin cytoskeletal rearrangements that result in the internalization of a large bacterial aggregate by the so-called 'invasome'. Later, infection studies with *bepC* deletion mutants and ectopic expression of BepC have implicated this effector in triggering an actin-dependent cell contractility phenotype characterized by fragmentation of migrating cells due to deficient rear detachment at the trailing edge, and BepE was shown to counterbalance this remarkable phenotype. However, the molecular mechanism of how BepC triggers cytoskeletal changes and the host factors involved remained elusive. Using infection assays, we show here that T4SS-mediated transfer of BepC is sufficient to trigger stress fiber formation in non-migrating epithelial cells and additionally cell fragmentation in migrating endothelial cells. Interactomic analysis revealed binding of BepC to a complex of the Rho guanine nucleotide exchange factor GEF-H1 and the serine/threonine-protein kinase MRCKα. Knock-out cell lines revealed that only GEF-H1 is required for mediating BepC-triggered stress fiber formation and inhibitor studies implicated activation of the RhoA/ROCK pathway downstream of GEF-H1. Ectopic co-expression of tagged versions of GEF-H1 and BepC truncations revealed that the C-terminal 'Bep intracellular delivery' (BID) domain facilitated anchorage of BepC to the plasma membrane, whereas the N-terminal 'filamentation induced by cAMP' (FIC) domain facilitated binding of GEF-H1. While FIC domains typically mediate post-translational modifications, most prominently AMPylation, a mutant with quadruple amino acid exchanges in the putative active site indicated that the BepC FIC domain acts in a non-catalytic manner to activate GEF-H1. Our data support a model in which BepC activates the RhoA/ROCK pathway by re-localization of GEF-H1 from microtubules to the plasma membrane.

Author summary

A wide variety of bacterial pathogens evolved numerous virulence factors to subvert cellular processes in support of a successful infection process. Likewise, bacteria of the genus

Bartonella translocate a cocktail of effector proteins (Beps) via a type-IV-secretion system into infected cells in order to interfere with host signaling processes involved in cytoskeletal dynamics, apoptosis control, and innate immune responses. In this study, we demonstrate that BepC triggers actin stress fiber formation and a linked cell fragmentation phenotype resulting from distortion of rear-end retraction during cell migration. The ability of BepC to induce actin stress fiber formation is directly associated with its ability to bind GEF-H1, an activator of the RhoA pathway that is sequestered in an inactive state when bound to microtubules but becomes activated upon release to the cytoplasm. Our findings suggest that BepC is anchored via its BID domain to the plasma membrane where it recruits GEF-H1 via its FIC domain, eventually activating the RhoA/ROCK signaling pathway and leading to stress fiber formation.

Introduction

The cytoskeleton plays major roles in epithelial and endothelial barrier integrity, pathogen uptake, and immune cell functions such as phagocytosis and cell migration. Depending on their infection strategies, pathogenic bacteria have evolved a plethora of virulence factors to obstruct or subvert these cytoskeletal functions. Many of these virulence factors target Rho family GTPases due to their central roles in regulating cytoskeletal dynamics. These virulence factors stimulate, attenuate or inactivate the intrinsic GTPase activities of Rho family GTPases, either directly through covalent modification [1], or indirectly by deregulating the activities of guanine nucleotide exchange factors (GEFs) [2] or GTPase-activating proteins (GAPs), or by molecular mimicry of GEF or GAP functions [3]. These virulence factors can be toxins, which are secreted to the extracellular milieu and are enabled to autonomously enter cells in order to reach their targets, or they are effector proteins, which are directly translocated into host cell via dedicated delivery devices, such as the type III (T3SS) or type IV (T4SS) secretion systems [4].

The gram-negative, facultative intracellular pathogens of the genus *Bartonella* are arthropod-borne bacteria that cause long-lasting intraerythrocytic bacteremia as hallmark of chronic infection in their specific mammalian reservoirs. While only few species are human-specific (e.g., *B. quintana*), many of the animal-specific species are zoonotic as they cause incidental human infections, resulting in a broad spectrum of clinical manifestations that ranges from asymptomatic courses to life-threatening disease [5]. For instance, the zoonotic pathogen *B. henselae* (*Bhe*) naturally infects cats, but is responsible for the majority of human cases of *Bartonella* infection due to transmission by cat scratch or bite. Infected immunocompetent individuals develop so-called cat scratch disease that leads to lymphadenopathy and fever, while immunocompromised patients develop bacillary angiomatosis characterized by vasoproliferative tumors of the skin and inner organs [6].

The *bartonellae* utilize a VirB/VirD4 T4SS to translocate a cocktail of *B*artonella effector proteins (Beps) into host cells, and their orchestrated activities modulate multiple cellular processes and thereby decisively contribute to the stealth infection strategy and capacity of these pathogens to cause chronic infection [6,7]. Beps are multi-domain proteins that share a common architecture at their C-terminus, which is composed of a 'Bep intracellular delivery' (BID) domain and a positively charged tail that together constitute an evolutionary conserved bipartite signal for T4SS-mediated translocation [8,9]. Despite their conserved fold [10], BID domains display significant variability in surface-exposed amino acids that facilitated the evolution of specific, non-enzymatic effector functions within host cells, e.g. by mediating

protein-protein interaction or anchorage to the plasma membrane [11–15]. The N-terminus is more divergent. It may encode additional BID domains [13,16], or tandem-repeated tyrosine phosphorylation motifs that serve as scaffolds for the assembly of signaling complexes [5,13,16–18], however, most Beps carry an N-terminal 'filamentation induced by cAMP" (FIC) domain and a central OB (oligosaccharide binding) fold [16]. This conserved FIC-OB--BID domain order is also considered to represent the architecture of the ancestral effector from which all present-day Beps have evolved by gene duplication, domain shuffling, and sequence diversification [16,17,19]. FIC domains are characterized by a core composed of six α-helices, which includes a signature sequence called 'FIC motif' and a so-called 'flap' sequence [20,21]. The canonical FIC motif HxFx(D/E)GNGRxxR plays a key role in the transfer of a phosphate-containing group onto the hydroxyl side chain of the amino acids threonine (T), serine (S), or tyrosine (Y) in target proteins. Most FIC domains mediate the transfer of an AMP moiety from ATP as substrate by a reaction known as AMPylation or adenylylation, however, some FIC proteins are able to utilize different substrates to catalyze other posttranslational modifications [20,21]. The flap of the FIC domain overlays the active site and mediates β-strand augmentation with the amino acid chain of target proteins to register a hydroxyl side-chain for modification [21,22]. The OB fold connects the N-terminal FIC domain and the C-terminal BID domain. It may primarily serve as an interdomain fold [23], but despite its small size it may extend a protein-protein interaction interface and/or effector localization sequence composed by the proximal FIC or BID domains.

The *Bartonella* effector protein C (BepC) was reported to trigger two distinct F-actin driven cytoskeletal processes that are both dependent on actin stress fiber formation and dynamics [7]. First, $BepC_{Bhe}$ was shown to act in concert with $BepF_{Bhe}$ in triggering pronounced actin cytoskeletal rearrangement in primary human umbilical vein endothelial cells (HUVECs) and epithelial HeLa cells that resulted in the internalization of a large bacterial aggregate by a multi-step process known as 'invasome-mediated internalization' [12,24–26]. Then, infection assays with $\Delta bepC_{Bhe}$ deletion mutants in dendritic cells and HUVECs and ectopic expression of mCherry-$BepC_{Bhe}$ in HUVECs implicated BepC in triggering actin stress fiber formation, resulting in the fragmentation of migratory cells due to deficient rear detachment at the trailing edge [11]. This remarkable phenotype based on imbalanced formation and disassembly of focal adhesion complexes during actomyosin-dependent cell contraction is at least in part antagonized by the activity of BepE [11]. On the structural level, BepC displays the ancestral FIC-OB-BID architecture. However, unlike most Fic proteins, BepC is characterized by a non-canonical but well conserved FIC motif (HxFx**K**GNGRxxR), which differs from the canonical motif by the replacement of an acidic residue (D/E) by a lysine (K). The crystal structure of the FIC domain of BepC from *Bartonella tribocorum* ($BepC_{Btr}$), co-crystallized with an ATP derivative in the active site, indicated that the lysine is directly interacting with the α- and β-phosphates of the ATP analog (PDB: 4WGJ), thus functionally replacing the magnesium cation (Mg^{2+}) that is coordinated by the acidic residue (D/E) of the canonical FIC motif [27]. Although this arrangement might be compatible with an AMP-transferase activity as shown for FIC domains with a conserved canonical FIC motif, no enzymatic activity has been reported yet for the BepC FIC domain. The BID domain of $BepC_{Bhe}$ was shown to mediate effector translocation via the VirB/VirD4 T4SS [8] and to associate with the plasma membrane within host cells [14]. Despite these insights from structure/function analysis, the molecular mechanism of how BepC triggers cytoskeletal changes that contribute to invasome formation and cell fragmentation of migratory cells remained elusive, and no host targets of BepC have been reported to date.

In this study, we demonstrate that BepC triggers actin stress fiber formation by activating the RhoA GTPase signaling cascade via recruitment of GEF-H1 to the plasma membrane. We

further show that BepC binds GEF-H1 via the FIC domain while anchorage to the plasma membrane depends on the BID domain.

Results

BepC triggers actin stress fiber formation and cell fragmentation in human umbilical vein endothelial cells

Infection with *Bhe* Δ*bepC*$_{Bhe}$ deletion mutants and ectopic expression of mCherry-BepC$_{Bhe}$ in HUVECs implicated BepC in triggering actin stress fiber formation and the linked cell fragmentation phenotype resulting from distorted rear-end detachment during cell migration [11]. To demonstrate that these prominent phenotypes can result from VirB/VirD4-dependent translocation of BepC$_{Bhe}$ into infected HUVECs, we expressed BepC$_{Bhe}$ with a N-terminal triple FLAG (Fig 1A) in the effector-free background of the *Bhe* Δ*bepA-G* strain [8]. Translocation of 3xFLAG-BepC$_{Bhe}$ by this strain triggered both F-actin-dependent phenotypes in dependency of infection time and multiplicity of infection (MOI) (Figs 1B and S1A), while the isogenic control strain containing the empty expression plasmid did not noticeably alter the F-actin cytoskeleton compared to uninfected cells (Figs 1B, S1A and S1B). BepC$_{Bhe}$-dependent actin stress fiber formation was evident at MOI of 200 at 24 h, while at this time-point cell fragmentation became only visible at MOI of 400. Generally, stress fiber formation and cell fragmentation phenotypes were more pronounced at 48 h than at 24 h, and this late time-point was thus used for most follow-up experiments. Of note, BepC-triggered cell fragmentation resulted in decreased cell number, while cellular fragments did not display morphological features of apoptosis (i.e., blebbing) or necrotic cell death (i.e., lysis).

The slow kinetics and high MOI-dependency of BepC$_{Bhe}$–triggered stress fiber formation suggest that the effector may act on its host target(s) by protein-protein interaction (e.g., by target sequestration or mislocalization) rather than by an enzymatic mechanism. While BepC contains a well-conserved FIC domain that typically catalyzes an enzymatic activity such as AMPylation [20], its FIC motif (HxFx**K**GNGRxxR) differs from the canonical FIC motif (HxFx**D/E**GNGRxxR), which is defined by essential amino acids in the active site of these AMP-transferases, in one amino acid position (D/E replaced by K) [16]. Despite this single amino acid exchange, the FIC domain of BepC might still harbor enzymatic activity; possibly one that differs from AMPylation. However, we reasoned that the mutations of this lysine and of three additional amino acids known to be essential for enzymatic activity in FIC domains with a canonical FIC motif [20,21,28] should incapacitate any presumable enzymatic activity of the BepC FIC domain. We thus constructed the quadruple mutant BepC$_{Bhe}^{****}$ with the amino acid exchanges H146A, K150A, R154A, R157A, resulting in a highly degenerated FIC motif (**A**xFx**A**GNG**A**xx**A,** Fig 1A). Moreover, we constructed another mutant that might compromise BepC-specific target modification by exchanging the flap region, which registers the target protein to the active site of FIC domains, between BepC$_{Bhe}$ and BepA$_{Bhe}$ (3xFLAG--BepC$_{Bhe}$(Flap BepA$_{Bhe}$), Fig 1A). Both of these BepC$_{Bhe}$ mutant proteins maintained the same capacity to trigger stress fiber formation and cell fragmentation as BepC$_{Bhe}$, indicating that BepC$_{Bhe}$ may not require enzymatic modification of host targets to trigger actin rearrangements (Fig 1B and 1D). However, deletion of the FIC domain (3xFLAG-BepC$_{Bhe}$(OB-BID), Fig 1A) rendered the truncated BepC$_{Bhe}$ protein unable to produce any phenotype (Fig 1B and 1D), despite being expressed as the same level as the wild-type and mutants versions of BepC$_{Bhe}$ (Fig 1C).

In summary, the FIC domain of BepC is required for actin stress fiber formation and cell fragmentation, but neither a conserved FIC motif nor a specific flap region are necessary, suggesting that the actin phenotype is linked to a non-enzymatic activity.

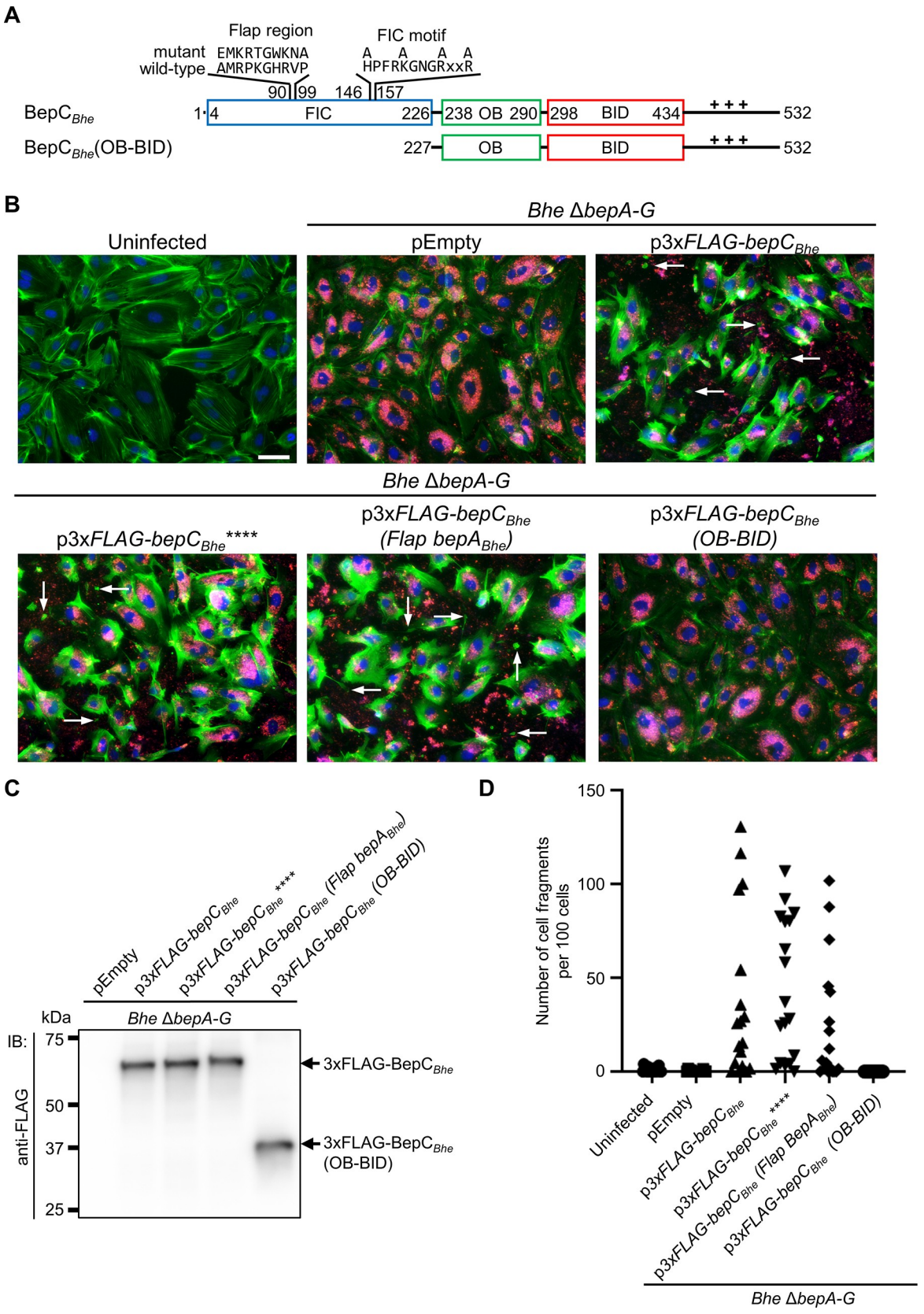
A
Flap region
FIC motif
mutant EMKRTGWKNA
wild-type AMRPKGHRVP
A A A A
HPFRKGNGRxxR
90 99 146 157
BepC$_{Bhe}$
1 4 FIC 226 238 OB 290 298 BID 434 +++ 532
BepC$_{Bhe}$(OB-BID)
227 OB BID +++ 532
B
Bhe ΔbepA-G
Uninfected
pEmpty
p3x*FLAG-bepC$_{Bhe}$*
Bhe ΔbepA-G
p3x*FLAG-bepC$_{Bhe}$*****
p3x*FLAG-bepC$_{Bhe}$* (Flap *bepA$_{Bhe}$*)
p3x*FLAG-bepC$_{Bhe}$* (OB-BID)
C
pEmpty
p3x*FLAG-bepC$_{Bhe}$*
p3x*FLAG-bepC$_{Bhe}$*****
p3x*FLAG-bepC$_{Bhe}$* (Flap *bepA$_{Bhe}$*)
p3x*FLAG-bepC$_{Bhe}$* (OB-BID)
kDa
Bhe ΔbepA-G
IB:
anti-FLAG
75
50
37
25
3xFLAG-BepC$_{Bhe}$
3xFLAG-BepC$_{Bhe}$ (OB-BID)
D
Number of cell fragments per 100 cells
150
100
50
0
Uninfected
pEmpty
p3x*FLAG-bepC$_{Bhe}$*
p3x*FLAG-bepC$_{Bhe}$*****
p3x*FLAG-bepC$_{Bhe}$* (Flap *BepA$_{Bhe}$*)
p3x*FLAG-bepC$_{Bhe}$* (OB-BID)
Bhe ΔbepA-G

Fig 1. The BepC$_{Bhe}$ FIC domain but not a conserved FIC motif or flap region is required for actin stress fiber formation in *B. henselae*-infected HUVECs. (**A**) Schematic view of BepC$_{Bhe}$ wild-type and mutant variants analyzed in this figure. The positively charged tail at the C-terminus is represented by +++. The N-terminally fused FLAG-tag triple copy (3xFLAG) is not shown. (**B**) HUVECs were infected at a multiplicity of infection (MOI) of 400 with isogenic *Bhe* Δ*bepA-G* strains expressing FLAG-tagged BepC$_{Bhe}$ wild-type or mutant versions, or carrying the empty plasmid. After 48 h of infection, cells were fixed and immunocytochemically stained, followed by fluorescence microscopy analysis. F-actin is represented in green, DNA in blue, and bacteria in red (scale bar = 50 μm). Arrows point to cell fragments resulting from distorted rear end retraction of migrating HUVEC. (**C**) Expression of 3xFLAG-tagged proteins was analyzed in bacterial lysates of indicated strains by immunoblot (IB) with an anti-FLAG antibody. (**D**) Cell fragmentation was quantified by manually analyzing 18 images, each containing around 100 cells, per condition. The graph shows the number of cell fragments per 100 cells. Shown are representative results from three independent experiments. BepC$_{Bhe}^{****}$ = BepC$_{Bhe}$ H146A, K150A, R154A, R157A; BepC$_{Bhe}$ (Flap BepA$_{Bhe}$) = BepC$_{Bhe}$ A90E, R92K, P93R, K94T, H96W, R97K, V98N, P99A.

https://doi.org/10.1371/journal.ppat.1008548.g001

BepC-triggered actin stress fiber formation in HeLa cells is dependent on both the FIC and the BID domain

To facilitate further cellular and molecular analysis of the mechanism underlying BepC-triggered actin stress fiber formation in an established cell line, we adopted the previously published HeLa cells infection model [25]. The capacity of isogenic strains expressing BepC$_{Bhe}$ wild-type and corresponding mutant variants to trigger actin stress fiber formation in HUVEC was fully reproduced in HeLa cells (Fig 2A and 2B). Additionally, staining infected HeLa cells with an anti-FLAG antibody confirmed the translocation of all BepC$_{Bhe}$ variants, excluding a translocation defect of BepC$_{Bhe}$ (OB-BID) (S2A Fig). The absence of actin stress fiber formation in HeLa cells infected with the translocation-deficient strain *Bhe* ΔbepA-G, ΔvirB4 expressing BepC definitely confirmed the T4SS dependency of the actin phenotype (S3 Fig).

As a complementary approach to VirB/VirD4-dependent effector translocation, we tested how ectopic expression of BepC$_{Bhe}$ wild-type and mutant variants affected actin stress fiber formation (Fig 3A). The phenotypic data and their quantification obtained for ectopic expression in HeLa cells (Fig 3B and 3D) are in full agreement with translocation-dependent infection phenotypes in both HUVEC and HeLa (Figs 1B, 2A and 2B). Importantly, the ectopic expression approach allowed us to test also a C-terminal truncation resulting in deletion of the entire BID domain and positively charged tail sequence (3xFLAG-BepC$_{Bhe}$(FIC-OB), Fig 3A) that could not be tested in the infection assay as deletion of this bipartite secretion signal abolishes VirB/VirD4-dependent protein translocation [8]. While being expressed at similar level to the wild-type effector (Figs 3C, and S2B), the lack of increased actin stress fiber formation by ectopic expression of this C-terminal truncation demonstrated the essential role of the BID domain in mediating this phenotype (Fig 3B and 3D).

The high level of sequence conservation of BepC homologs in different *Bartonella* species is indicative of a conserved molecular function [16]. We thus tested whether the capacity of BepC$_{Bhe}$ to trigger actin stress fiber formation is conserved among BepC homologs. HeLa cells were infected with *Bhe* Δ*bepA-G* expressing FLAG-tagged BepC of *Bhe*, *B. quintana* (*Bqu*), *B. tribocorum* (*Btr*), *B. taylorii* (*Bta*), or *B. grahamii* (*Bgr*). Increased F-actin stress fiber formation was evident for all BepC homologs, except for BepC$_{Bgr}$ that was highly similar to the negative control strain *Bhe* Δ*bepA-G* pEmpty (S4A and S4C Fig), likely as the result of the low expression level (S4B Fig). However, ectopic expression of these natural BepC variants demonstrated strongly increased stress fiber formation for each of them, including BepC$_{Bgr}$ (S4D, S4E and S4F Fig), suggesting that the lack of phenotype for BepC$_{Bgr}$ in the infection assay was indeed a false-negative result.

In summary, our data demonstrate that both FIC and BID domains are required for BepC-triggered actin stress fiber formation. Moreover, these actin rearrangements are triggered by all tested BepC homologs from various *Bartonella* species, suggesting that this conserved

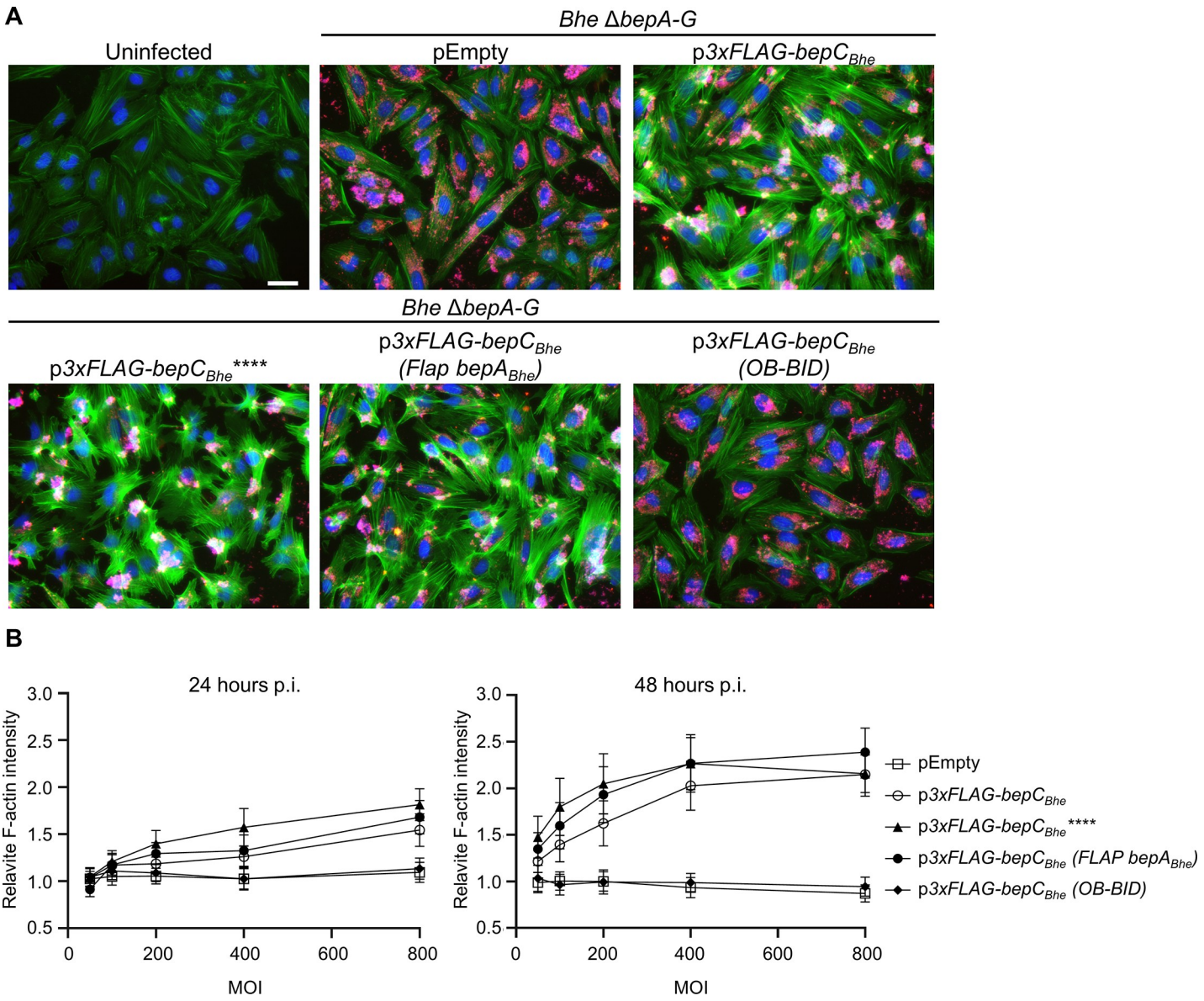

Fig 2. The BepC$_{Bhe}$ FIC domain but not a conserved FIC motif or flap region is required for actin stress fiber formation in *B. henselae*-infected HeLa cells. (**A**) HeLa cells were infected with isogenic *Bhe* Δ*bepA-G* strains expressing 3xFLAG-tagged BepC$_{Bhe}$ wild-type or mutant versions or carrying the empty plasmid at a multiplicity of infection (MOI) of 400. After 48 h of infection, cells were fixed and immunocytochemically stained, followed by fluorescence microscopy analysis. F-actin is represented in green, DNA in blue, and bacteria in red (scale bar = 50 μm). (**B**) HeLa cells were infected with the same strains as in (A) at MOI 50, 100, 200, 400, and 800, fixed after 24 h and 48 h and stained for F-actin. The graphs show the relative mean fluorescence intensity of the F-actin signal at 24 h (left panel) and 48 h (right panel) infection for the indicated MOIs normalized to the uninfected control. Shown are representative results from three independent experiments. BepC$_{Bhe}^{****}$ = BepC$_{Bhe}$ H146A, K150A, R154A, R157A; BepC$_{Bhe}$ (Flap BepA$_{Bhe}$) = BepC$_{Bhe}$ A90E, R92K, P93R, K94T, H96W, R97K, V98N, P99A.

https://doi.org/10.1371/journal.ppat.1008548.g002

effector function targeting the actin cytoskeleton is likely playing a crucial role during *Bartonella* infection.

GEF-H1 and MRCKα form a complex that co-immunoprecipitates with BepC

In order to search for potential host targets of BepC$_{Bhe}$, we identified interacting host proteins by an interactomics approach. To this end, we infected HeLa cells with *Bhe* Δ*bepA-G* expressing triple FLAG-tagged BepC$_{Bhe}$ or the isogenic strain containing the empty expression

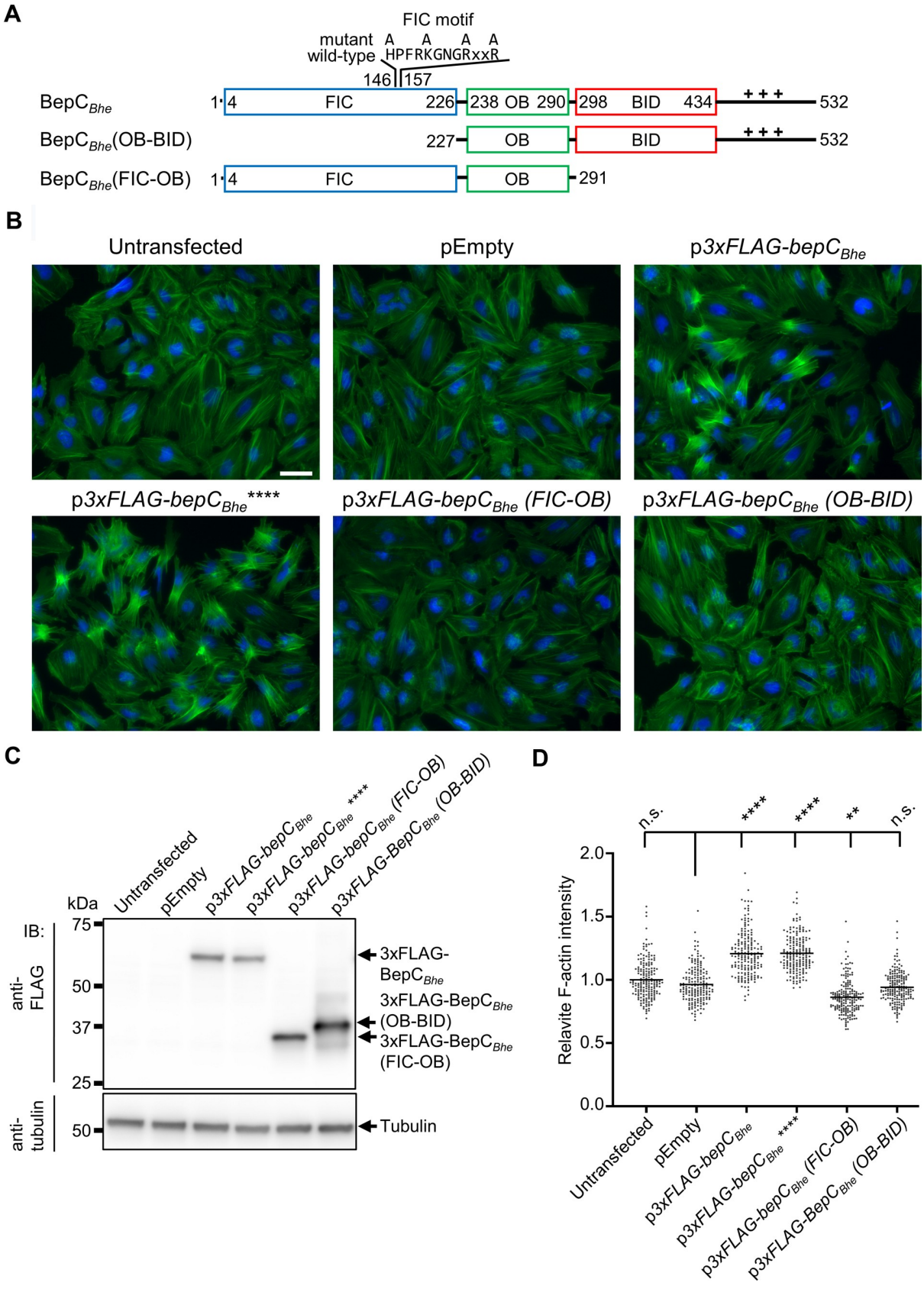
A
FIC motif
mutant A A A A
wild-type HPFRKGNGRxxR
146 157
BepC$_{Bhe}$ 1 4 FIC 226 238 OB 290 298 BID 434 +++ 532
BepC$_{Bhe}$(OB-BID) 227 OB BID +++ 532
BepC$_{Bhe}$(FIC-OB) 1 4 FIC OB 291
B
Untransfected
pEmpty
p3xFLAG-bepC$_{Bhe}$
p3xFLAG-bepC$_{Bhe}$ ****
p3xFLAG-bepC$_{Bhe}$ (FIC-OB)
p3xFLAG-bepC$_{Bhe}$ (OB-BID)
C
kDa
IB:
anti-FLAG
anti-tubulin
75
50
37
25
50
3xFLAG-BepC$_{Bhe}$
3xFLAG-BepC$_{Bhe}$ (OB-BID)
3xFLAG-BepC$_{Bhe}$ (FIC-OB)
Tubulin
D
Relavite F-actin intensity
2.0
1.5
1.0
0.5
0.0
n.s.
****
****
**
n.s.
Untransfected
pEmpty
p3xFLAG-bepC$_{Bhe}$
p3xFLAG-bepC$_{Bhe}$ ****
p3xFLAG-bepC$_{Bhe}$ (FIC-OB)
p3xFLAG-BepC$_{Bhe}$ (OB-BID)

Fig 3. Both FIC and BID domains are required for $BepC_{Bhe}$–triggered actin stress fiber formation upon ectopic effector expression in HeLa cells. (**A**) Schematic view of $BepC_{Bhe}$ wild-type and mutant variants analyzed in this figure. The positively charged tail at the C-terminus is represented by +++. The N-terminally fused triple FLAG-tag (3xFLAG) is not shown. (**B**) HeLa cells were transfected with the indicated plasmids for expression of 3xFLAG-tagged $BepC_{Bhe}$ wild-type, mutant versions, or truncations, or no protein as negative control (pEmpty). 24 h after transfection, cells were fixed and immunocytochemically stained, followed by fluorescence microscopy analysis. F-actin is represented in green and DNA in blue (scale bar = 50 μm). (**C**) Expression of FLAG-tagged proteins was analysed in cell lysates by immunoblot with an anti-FLAG antibody. (**D**) The mean fluorescence intensity of F-actin shown for conditions shown in (B) was quantified for 74 imaged sites using CellProfiler. Data are represented as dot plots with each data point corresponding to the average of all mean cell intensity values within one imaged site. Statistical significance was determined using Kruskal-Wallis test (**** corresponds to p-value ≤ 0.0001). $BepC_{Bhe}{}^{****}$ = $BepC_{Bhe}$ H146A, K150A, R154A, R157A.

https://doi.org/10.1371/journal.ppat.1008548.g003

plasmid. Following cell lysis, 3xFLAG-$BepC_{Bhe}$ was pulled down with anti-FLAG-tag antibodies and co-immunoprecipitating host proteins were identified by mass spectrometry (Fig 4A and S1 Table). Compared to the negative control, six proteins showed an increase of at least 8-fold and a q-value lower than 0.05 (Fig 4A). Three of these six proteins were identified by a single peptide. These proteins were not followed up as their relevance was uncertain. As expected, one of the three remaining proteins corresponded to $BepC_{Bhe}$ as the bait. The two outstanding interactors, GEF-H1 and MRCKα, were particularly interesting as both are involved in regulating F-actin rearrangements (Fig 4B). On one hand, GEF-H1 promotes the activation of RhoA by exchanging GDP for GTP, which then via ROCK activation and subsequent phosphorylation of myosin light chain (MLC) ultimately leads to actin stress fiber formation [28–31]. On the other hand, MRCKα is a downstream effector of the Cdc42 pathway and directly phosphorylates MLC and, as ROCK, inhibits the myosin light chain phosphatase (MLCP), thereby promoting actin stress fiber formation as well [29–31].

To validate the $BepC_{Bhe}$ interaction with GEF-H1 and MRCKα as identified by interactomics in HeLa cells, we performed a reciprocal co-immunoprecipitation experiment in a different cell type. To this end, HUVECs were infected with *Bhe* Δ*bepA-G* expressing FLAG-tagged $BepC_{Bhe}$ or carrying the empty expression plasmid. Following pull-down of GEF-H1 or MRCKα (Fig 4C), 3xFLAG-$BepC_{Bhe}$ was detected in both pull-down fractions, confirming that the three proteins are part of a complex. In contrast, 3xFLAG-$BepC_{Bhe}$ (OB-BID) did not co-immunoprecipitate with either GEF-H1 or MRCKα, indicating that the FIC domain is critical for this interaction. Moreover, even in the absence of $BepC_{Bhe}$, GEF-H1 co-immunoprecipitated with MRCKα and vice versa, indicating that MRCKα and GEF-H1 are part of a native complex that to our knowledge has not been described yet (Fig 4C).

In summary, interactomics identified a native complex of GEF-H1 and MRCKα that co-immunoprecipitated with $BepC_{Bhe}$, leaving it open whether BepC interacts in a direct manner with GEF-H1, or with MRCKα, or with both.

The interaction of GEF-H1 with BepC is independent of MRCKα

To untangle the molecular interactions within the complex of BepC, GEF-H1, and MRCKα, we generated HeLa knock-out cell lines for GEF-H1 or MRCKα by CRISPR/Cas9 gene editing. To this end, we co-transfected HeLa cells with two different plasmids encoding Cas9 and sgRNAs that are specific to either the first or the last exon of the gene of interest. Following selection and polyclonal expansion of knock-out cells, we tested expression of GEF-H1 or MRCKα via immunoblot analysis. The data indicate a complete knock-out for MRCKα, and a partial knock-out for GEF-H1 with a nevertheless strongly diminished protein level compared to the parental wild-type cell line (Figs 4D and 5B).

The established knock-out cell lines for GEF-H1 or MRCKα and the parental wild-type cell line were then used to unravel the interaction between these cellular proteins and BepC by using infection and co-immunoprecipitation analysis. To this end, the two knock-out and the

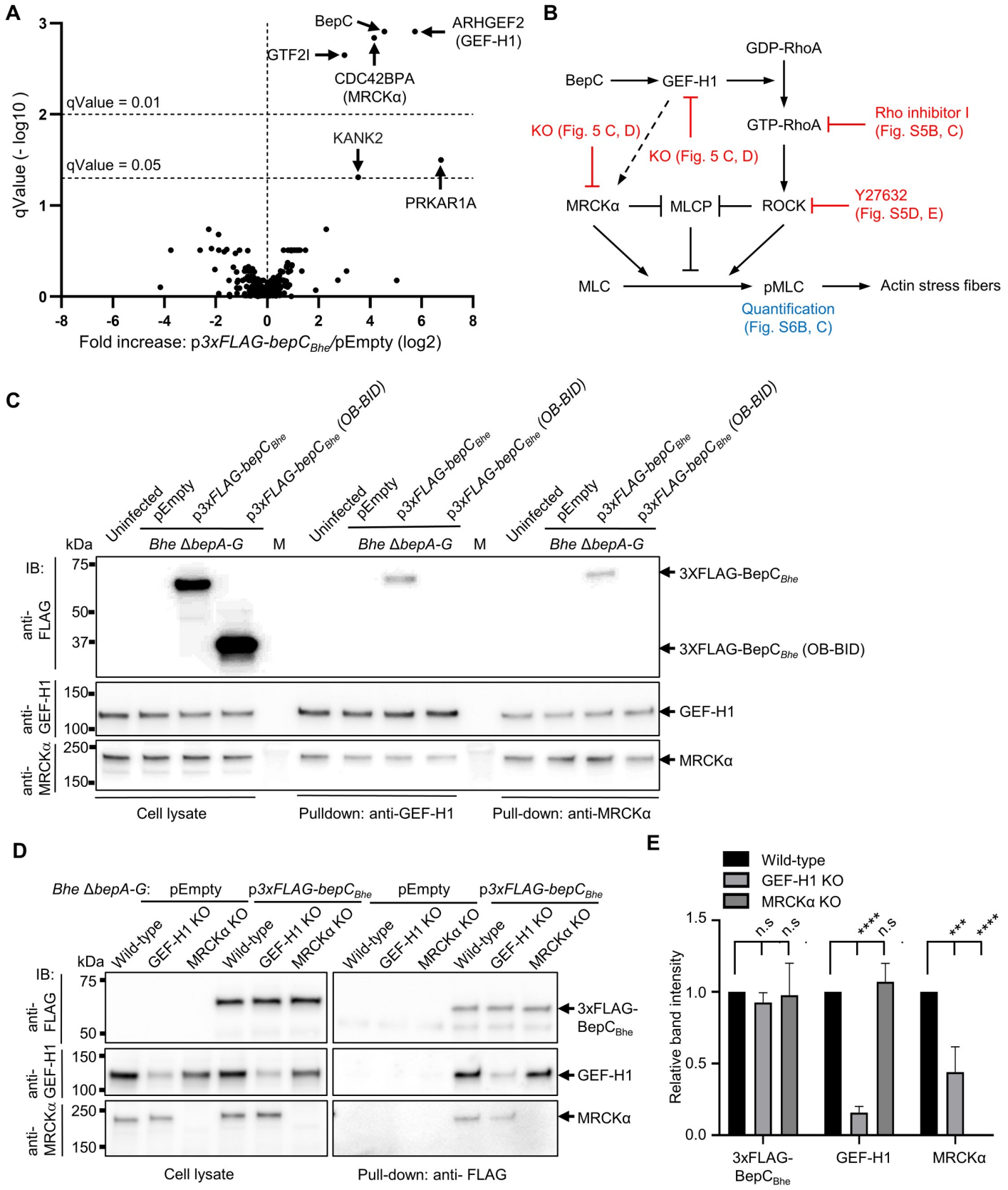
A
BepC
ARHGEF2 (GEF-H1)
GTF2I
CDC42BPA (MRCKα)
qValue = 0.01
KANK2
qValue = 0.05
PRKAR1A
qValue (- log10)
Fold increase: p3xFLAG-bepC$_{Bhe}$/pEmpty (log2)
B
GDP-RhoA
BepC
GEF-H1
GTP-RhoA
Rho inhibitor I (Fig. S5B, C)
KO (Fig. 5 C, D)
KO (Fig. 5 C, D)
MRCKα
MLCP
ROCK
Y27632 (Fig. S5D, E)
MLC
pMLC
Actin stress fibers
Quantification (Fig. S6B, C)
C
Uninfected
pEmpty
p3xFLAG-bepC$_{Bhe}$
p3xFLAG-bepC$_{Bhe}$ (OB-BID)
kDa
Bhe ΔbepA-G
M
IB:
anti-FLAG
anti-GEF-H1
anti-MRCKα
3XFLAG-BepC$_{Bhe}$
3XFLAG-BepC$_{Bhe}$ (OB-BID)
GEF-H1
MRCKα
Cell lysate
Pulldown: anti-GEF-H1
Pull-down: anti-MRCKα
D
Bhe ΔbepA-G:
pEmpty
p3xFLAG-bepC$_{Bhe}$
Wild-type
GEF-H1 KO
MRCKα KO
3xFLAG-BepC$_{Bhe}$
Cell lysate
Pull-down: anti- FLAG
E
Wild-type
GEF-H1 KO
MRCKα KO
Relative band intensity
n.s
****
***
3xFLAG-BepC$_{Bhe}$
GEF-H1
MRCKα

Fig 4. BepC$_{Bhe}$ binds to GEF-H1 and MRCKα. (**A**) HeLa cells were infected with *Bhe* Δ*bepA-G* expressing FLAG-tagged BepC$_{Bhe}$, or carrying the empty plasmid as a negative control, at MOI of 200. After 24 h of infection, cells were lysed and the lysate incubated in presence of anti-FLAG antibody. 3xFLAG-BepC$_{Bhe}$ and interacting proteins were pulled-down with protein G agarose beads and bound proteins were released with SDS-containing buffer. Samples (technical triplicates) were analyzed by mass spectrometry and data obtained for 3xFLAG-BepC$_{Bhe}$ and the negative control were compared (see S1 Table for a listing of all identified proteins). (**B**) Proposed model of BepC-triggered actin stress fiber formation with reference to the experimental data presented for validation. (**C**) HUVECs were infected with *Bhe* Δ*bepA-G* expressing 3xFLAG-tagged BepC$_{Bhe}$ or carrying empty plasmid at MOI of 200 for 24 h. Cells were lysed and incubated in presence of anti-GEF-H1 antibody or anti-MRCKα antibody. Antibody-bound proteins were subsequently pulled-down with protein G agarose beads, followed by elution with SDS-containing buffer. Cell lysates before pull-down and pull-down samples were analyzed by immunoblot using antibodies against FLAG-tag, GEF-H1, or MRCKα. (**D**) HeLa wild-type or knocked-out cells for GEF-H1 or MRCKα were infected with *Bhe* Δ*bepA-G* expressing FLAG-tagged BepC$_{Bhe}$ or carrying the empty plasmid as a negative control at MOI of 200. After 24 h of infection, cells were lysed and incubated with anti-FLAG antibodies. 3xFLAG-BepC$_{Bhe}$ was pulled-down with protein G agarose beads before eluted with SDS. Cell lysates before pull-down and pull-down samples were analyzed by immunoblot against FLAG-tag, GEF-H1, or MRCKα. (**E**) Pull-down fractions of three independent experiments samples as shown in (D) were quantified using ImageJ and plotted as relative intensities of the bands normalized to the wild-type control. Shown are representative results from three independent experiments.

https://doi.org/10.1371/journal.ppat.1008548.g004

parental cell lines were infected with *Bhe* Δ*bepA-G* expressing FLAG-tagged BepC$_{Bhe}$ or carrying the empty expression plasmid. Following cell lysis, 3xFLAG-BepC$_{Bhe}$ was pulled-down and tested for co-immunoprecipitation of GEF-H1 and/or MRCKα by immunoblot analysis (Fig 4D). GEF-H1 interaction with 3xFLAG-BepC$_{Bhe}$ was indistinguishable for wild-type cells and MRCKα knock-out cells, indicating that the interaction is independent of MRCKα (Fig 4D, pull-down and Fig 4E). In contrast, MRCKα interaction with 3xFLAG-BepC$_{Bhe}$ was reduced by about 60% in the partial GEF-H1 knock-out cell line compared to wild-type cells (Fig 4D, pull-down and Fig 4E), suggesting that this interaction is at least in part dependent on GEF-H1. Clarification of this finding may require the establishment of a complete GEF-H1 knock-out cell line, which, however, may not be viable.

Overall, our data indicate that the interaction of BepC$_{Bhe}$ with GEF-H1 is independent of MRCKα, while the interaction with MRCKα depends at least partially on GEF-H1.

BepC–triggered actin stress fiber formation requires GEF-H1 and is associated with GEF-H1 relocalization

Next, we used the established GEF-H1 or MRCKα knock-out cells and parental wild-type cells in infection experiments to test for the roles of GEF-H1 and MRCKα in mediating BepC$_{Bhe}$–triggered stress fiber formation (Fig 5A). To this end, we infected these three cell lines with *Bhe* Δ*bepA-G* expressing FLAG-tagged BepC$_{Bhe}$ or carrying the empty expression plasmid, or left them uninfected as an additional negative control. Staining for F-actin unequivocally demonstrated that GEF-H1 is essential for mediating BepC$_{Bhe}$–triggered stress fiber formation, while MRCKα is neglectable for this process (Fig 5C and 5D). Strikingly, staining with anti-GEF-H1 antibodies provided first evidence for a BepC–dependent relocalization of GEF-H1 (Fig 5E). The GEF-H1 knock-out cells displayed invariant background staining for all three conditions. However, parental wild-type and MRCKα knock-out cells displayed a characteristic cytoplasmic GEF-H1 staining pattern consistent with microtubular association in both uninfected and control infection conditions. In contrast, GEF-H1 seemed to relocalize to the plasma membrane upon infection with the FLAG-tagged BepC$_{Bhe}$ expressing strain (Fig 5E).

In summary, we demonstrated an essential role of GEF-H1 for BepC$_{Bhe}$–dependent actin stress fiber formation and provided first indications that BepC$_{Bhe}$ translocation mediates a relocalization of GEF-H1 from a canonical microtubular-association to a putative plasma membrane localization.

BepC interacts with GEF-H1 via its FIC domain while plasma membrane association is mediated by the BID domain

To substantiate our findings on a BepC-dependent relocalization of GEF-H1 from microtubules to the plasma membrane and to determine which BepC domain interactions are involved

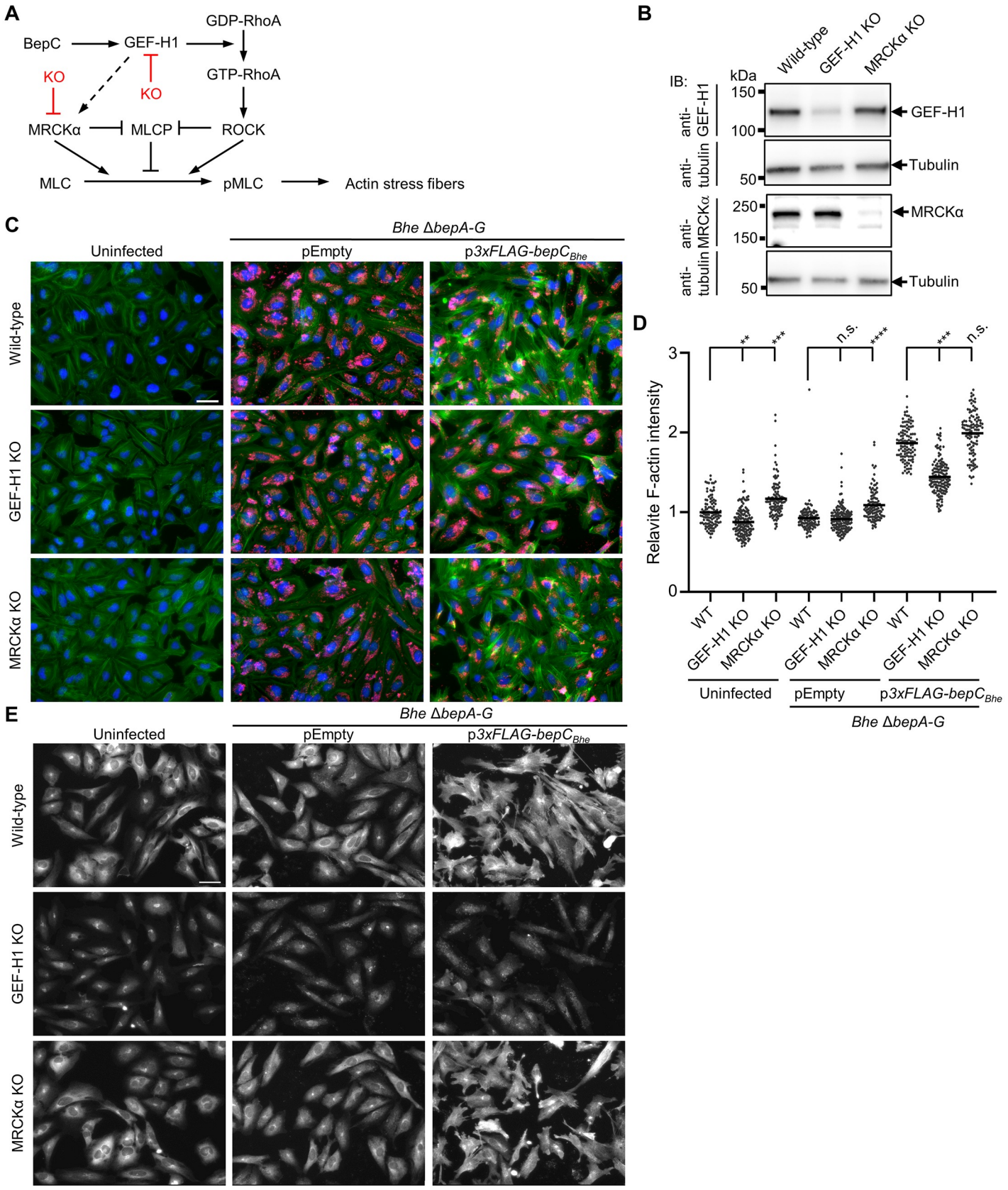
A
BepC
GEF-H1
GDP-RhoA
GTP-RhoA
KO
KO
MRCKα
MLCP
ROCK
MLC
pMLC
Actin stress fibers
B
Wild-type
GEF-H1 KO
MRCKα KO
IB:
kDa
anti-GEF-H1
150
100
GEF-H1
anti-tubulin
50
Tubulin
anti-MRCKα
250
150
MRCKα
anti-tubulin
50
Tubulin
C
Bhe ΔbepA-G
Uninfected
pEmpty
p3xFLAG-bepC Bhe
Wild-type
GEF-H1 KO
MRCKα KO
D
Relavite F-actin intensity
3
2
1
0
**
***
n.s.
****
***
n.s.
WT
GEF-H1 KO
MRCKα KO
Uninfected
pEmpty
p3xFLAG-bepC Bhe
Bhe ΔbepA-G
E
Bhe ΔbepA-G
Uninfected
pEmpty
p3xFLAG-bepC Bhe
Wild-type
GEF-H1 KO
MRCKα KO

Fig 5. GEF-H1 is essential for BepC$_{Bhe}$–triggered actin stress fiber formation while MRCKα is dispensable. (A) Proposed model of BepC-triggered actin stress fiber formation with indication of the GEF-H1 and MRCKα knock-out. (B) HeLa cells were co-transfected with two different plasmids encoding Cas9 and a sgRNA, specific either to the first or the last exon of the target gene (GEF-H1 or MRCKα). After selection and expansion of transfected cells, expression of GEF-H1 or MRCKα was tested by immunoblot analysis. Tubulin was used as loading control. (C-E) HeLa cells wild-type, GEF-H1 KO, and MRCKα KO were infected with *Bhe* Δ*bepA-G* expressing FLAG-tagged BepC$_{Bhe}$, or carrying the empty plasmid as a negative control, at MOI of 400. After 48 h of infection, cells were fixed, stained by immunocytochemistry and analyzed by fluorescence microscopy. (C) F-actin is represented in green, DNA in blue, and bacteria in red. (D) The mean fluorescence intensity of F-actin for conditions shown in (C) was quantified for 111 imaged sites using CellProfiler. Data are represented as dot plots with each data point corresponding to the average of all mean cell intensity values within one imaged site normalized to the uninfected wild-type (WT) control. Statistical significance was determined using Kruskal-Wallis test (**** corresponds to p-value $\leq$ 0.0001). (E) Anti-GEF-H1 staining is represented in white (scale bar = 50 μm). Shown are representative results from three independent experiments.

https://doi.org/10.1371/journal.ppat.1008548.g005

in mediating this effect, we have used an ectopic co-expression approach in HeLa cells. To follow GEF-H1 localization, we expressed a functional eGFP-GEF-H1 fusion that was previously reported to localize primarily to microtubules, indistinguishably from endogenous GEF-H1 [32]. Co-transfection with an empty expression plasmid (pEmpty) confirmed this canonical staining pattern as demonstrated by colocalization with microtubules (Fig 6A). However, co-expression with Flag-tagged BepC$_{Bhe}$ showed that, while a part of the GEF-H1 signal remained associated with microtubules, a significant proportion of the eGFP-GEF-H1 signal co-localized with 3xFLAG-BepC$_{Bhe}$ at the plasma membrane (Fig 6B, upper panel of x-y projections and left panel of x-z sections). In sharp contrast, the microtubule-associated localization of eGFP--GEF-H1 was unperturbed when co-expressed with either 3xFLAG-BepC$_{Bhe}$(FIC-OB) or 3xFLAG-BepC$_{Bhe}$(OB-BID) truncation constructs (Fig 6B, middle or lower panel of x-y projections or middle or right panel of x-z sections, respectively). Strikingly, 3xFLAG-BepC$_{Bhe}$(FIC-OB) colocalized with both eGFP-GEF-H1 and microtubules (Fig 6B, middle panels of x-y projections and x-z sections), indicating that the soluble FIC-OB fragment binds to GEF-H1 without dissociating it from microtubules. On the contrary, 3xFLAG-BepC$_{Bhe}$(OB-BID) displayed a plasma membrane localization without any sign of co-localization with microtubule-bound eGFP-GEF-H1 (Fig 6B, lower panel of x-y projections and right panel of x-z sections).

To further corroborate these findings on BepC domain-specific interaction with GEF-H1 or association to the plasma membrane derived by fluorescent microscopy, we performed complementary pull-down assays and subcellular fractionation analysis (Fig 7). By pulling-down 3xFLAG-tagged BepC$_{Bhe}$ or the FIC-OB or OB-BID truncation derivatives in Hela cells, we could demonstrate that endogenous GEF-H1 preferentially co-immunoprecipitate with the full-length BepC$_{Bhe}$, despite being less expressed. Additionally, BepC$_{Bhe}$ FIC-OB also showed a discrete but apparent binding of endogenous GEF-H1 while BepC$_{Bhe}$ OB-BID construct did not show any interaction (Fig 7A, right half of immunoblots). A corresponding pull-down experiment with HeLa cells ectopically expressing eGFP-GEF-H1 confirmed the findings with endogenous GEF-H1 by showing co-immunoprecipitation of eGFP-GEF-H1 with full-length BepC$_{Bhe}$ and FIC-OB constructs, while in comparison the OB-BID construct displayed only minute amounts of co-immunoprecipitating eGFP-GEF-H1 (Fig 7A, left half of immunoblots), demonstrating that ectopically expressed eGFP-GEF-H1, as also used in the microscopic analysis in Fig 6, behaves similarly than endogenous GEF-H1 regarding the specific interaction with BepC$_{Bhe}$ via its FIC domain. Next, we used subcellular fractionation to test for the localization of 3xFLAG-tagged BepC$_{Bhe}$ or its FIC-OB or OB-BID truncation derivatives. HeLa cells expressing either one of these constructs were ruptured and the full lysate was fractionated in the cytosolic and membrane fraction by ultracentrifugation. Fig 7B shows that the BepC$_{Bhe}$ full-length construct was entirely fractionating with membranes. The OB-BID construct was as well found primarily in the membrane fraction with only minute amounts in the cytosol, while in sharp contrast the FIC-OB construct was predominately present in the cytoplasmic fraction with scarce amounts fractioning to membranes. Due to the disassembly of

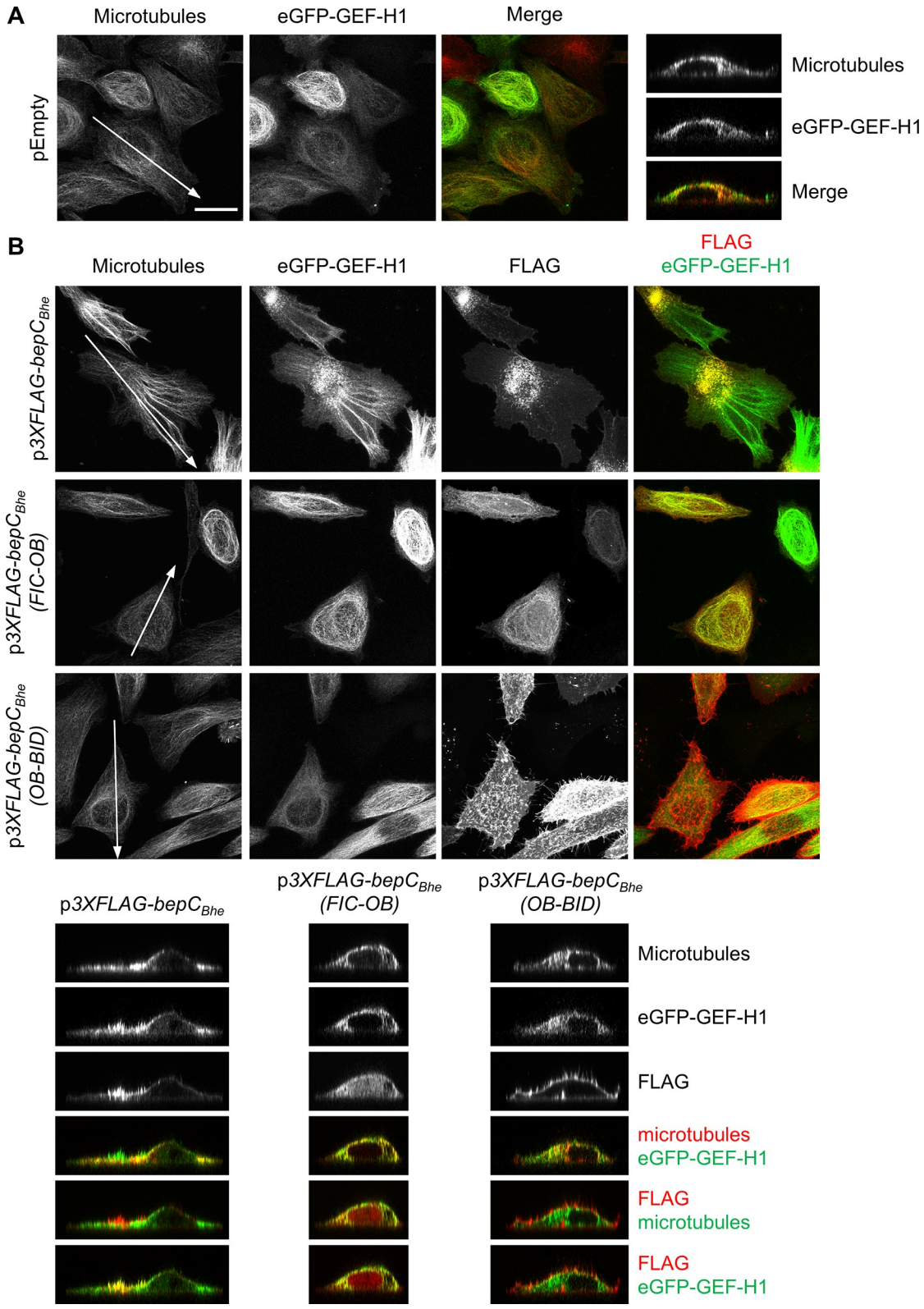

Fig 6. BepC$_{Bhe}$ recruits eGFP-GEF-H1 to the plasma membrane via binding of the FIC-OB domain to eGFP-GEF-H1 and binding of the BID domain to the plasma membrane shown by immunocytochemistry. (**A**-**B**) HeLa cells were co-transfected with an expression plasmid for eGFP-GEF-H1 and the indicated plasmids for either (**A**) no expression or (**B**) expression of either

3xFLAG-BepC$_{Bhe}$, 3xFLAG-BepC$_{Bhe}$(FIC-OB), or 3xFLAG-BepC$_{Bhe}$(OB-BID). After 24 h, cells were fixed and stained by immunofluorescence labeling for FLAG and microtubule before being analyzed by fluorescence microscopy (scale bar = 25 μm). The x-z sections presented correspond to orthogonal cuts at the white lines displayed in the microtubule channel.

https://doi.org/10.1371/journal.ppat.1008548.g006

microtubuli during cell rupture, GEF-H1 was found to localize predominately to the membrane fraction, which did not allow to test for its localization based on interaction with the three BepC$_{Bhe}$ constructs.

Taken together, the orthogonal data obtained from three different assays are fully consistent in indicating that the FIC domain and possibly the OB fold is required for BepC binding to GEF-H1, while the BID domain and possibly the OB fold is necessary for plasma membrane interaction. Together, we conclude that these domain interactions mediate the BepC-dependent relocalization of GEF-H1 from the canonical microtubule-association to the plasma membrane.

BepC-triggers actin stress fiber formation via the GEF-H1/RhoA/ROCK/pMLC pathway

While GEF-H1 binds to microtubules in an inactive conformation it gains GEF activity in association with membranes [32,33], where it activates either RhoA or Rac1 [34]. BepC-mediated recruitment of GEF-H1 to the plasma membrane should thus activate the RhoA and/or Rac1 pathway. Given that the RhoA pathway triggers stress fiber formation, while the Rac1 leads to lamellipodia formation [35], we reasoned that BepC/GEF-H1-mediated stress fiber formation is dependent on the RhoA pathway. To demonstrate this experimentally, we tested the involvement of components of the RhoA pathway in the BepC-triggered phenotype, i.e., by inhibiting RhoA or the Rho-kinase ROCK, and by evaluating the phosphorylation of the ROCK-substrate myosin light chain (pMLC) (S5A and S6A Figs). Rho inhibitor I, which inactivates RhoA, RhoB and RhoC in living cells [36], was found to interfere with stress fiber formation mediated by 3xFLAG-BepC$_{Bhe}$ in a concentration dependent manner (S5B and S5C Fig). Similarly, Y-27632, which inhibits ROCK in living cells [37], inhibited stress fiber formation by 3xFLAG-BepC$_{Bhe}$ in a concentration-dependent manner (S5D and S5E Fig). Finally, phosphorylation levels of MLC correlated with stress fiber formation triggered by 3xFLAG--BepC$_{Bhe}$ and active mutant constructs (S6B and S6C Fig).

Taken together, these data indicate that BepC activates a GEF-H1/RhoA/ROCK/pMLC signaling pathway in order to trigger actin stress fiber formation.

Discussion

Manipulation of the host cell actin cytoskeleton is crucial for many bacterial pathogens in order to cross epithelial or endothelial barriers, to disseminate into deeper tissue sites, to invade non-phagocytic cells, or to prevent phagocytosis by professional phagocytes [38]. These pathogens have evolved numerous toxins and effector proteins that interfere with actin cytoskeletal dynamics, typically by modulating the activities of Rho GTPases. Frontal-attack pathogens that cause acute infection often encode potent virulence factors that target the entire cellular pool of Rho GTPases by covalent modification or via molecular mimicry of GEFs or GAPs [3]. In contrast, pathogens causing chronic infections may selectively target subsets of Rho GTPases, e.g. by modulating the activity of one of the many endogenous GEFs or GAPs that usually control the activity of only a small subset of Rho GTPases in a temporal and spatial manner, thereby mediating rather subtle cytoskeletal changes that are more compatible with their stealth-attack infection strategy [3]. Here, we demonstrate a new mechanism of targeted

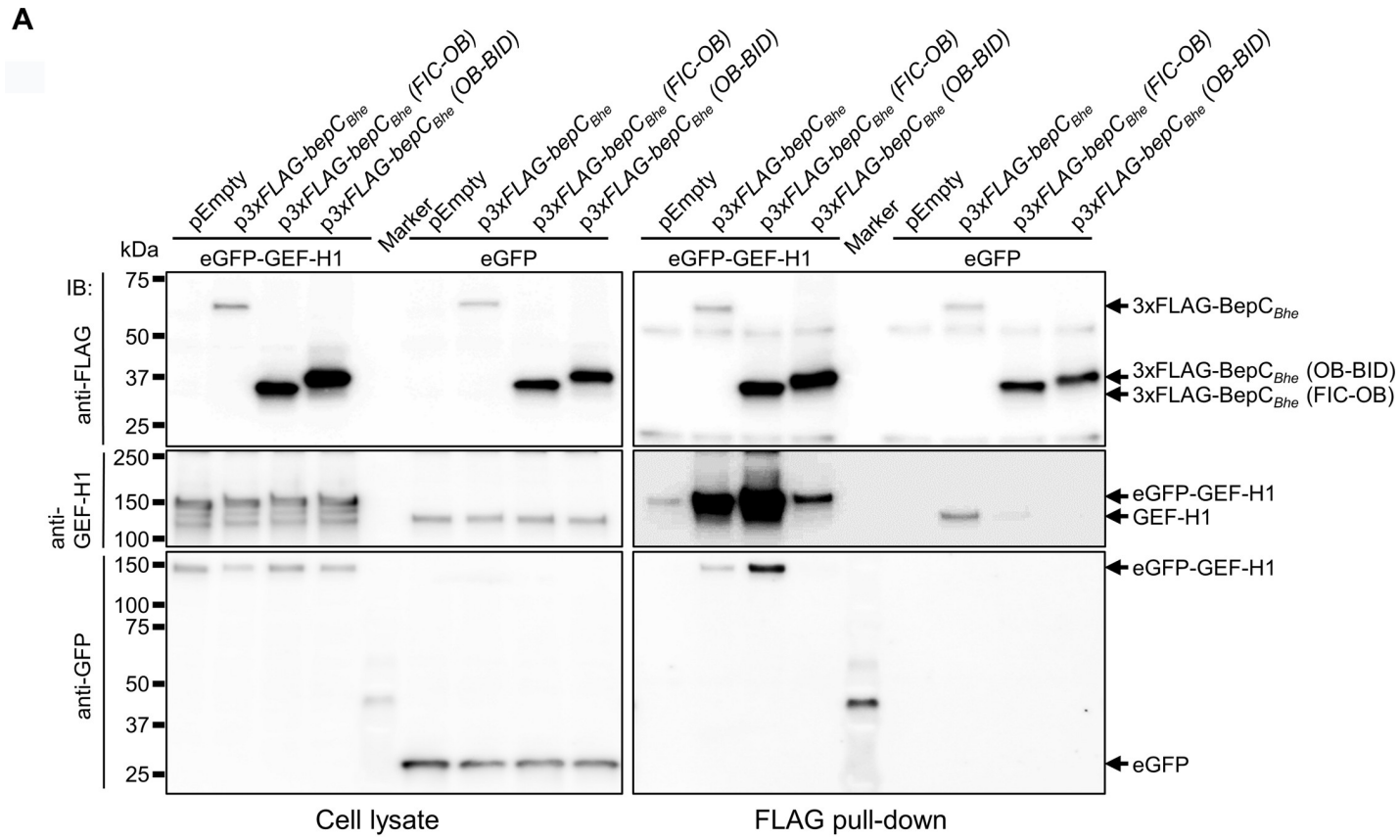
A
pEmpty
p3xFLAG-bepC$_{Bhe}$
p3xFLAG-bepC$_{Bhe}$ (FIC-OB)
p3xFLAG-bepC$_{Bhe}$ (OB-BID)
Marker
kDa
eGFP-GEF-H1
eGFP
IB:
anti-FLAG
anti-GEF-H1
anti-GFP
3xFLAG-BepC$_{Bhe}$
3xFLAG-BepC$_{Bhe}$ (OB-BID)
3xFLAG-BepC$_{Bhe}$ (FIC-OB)
eGFP-GEF-H1
GEF-H1
eGFP
Cell lysate
FLAG pull-down

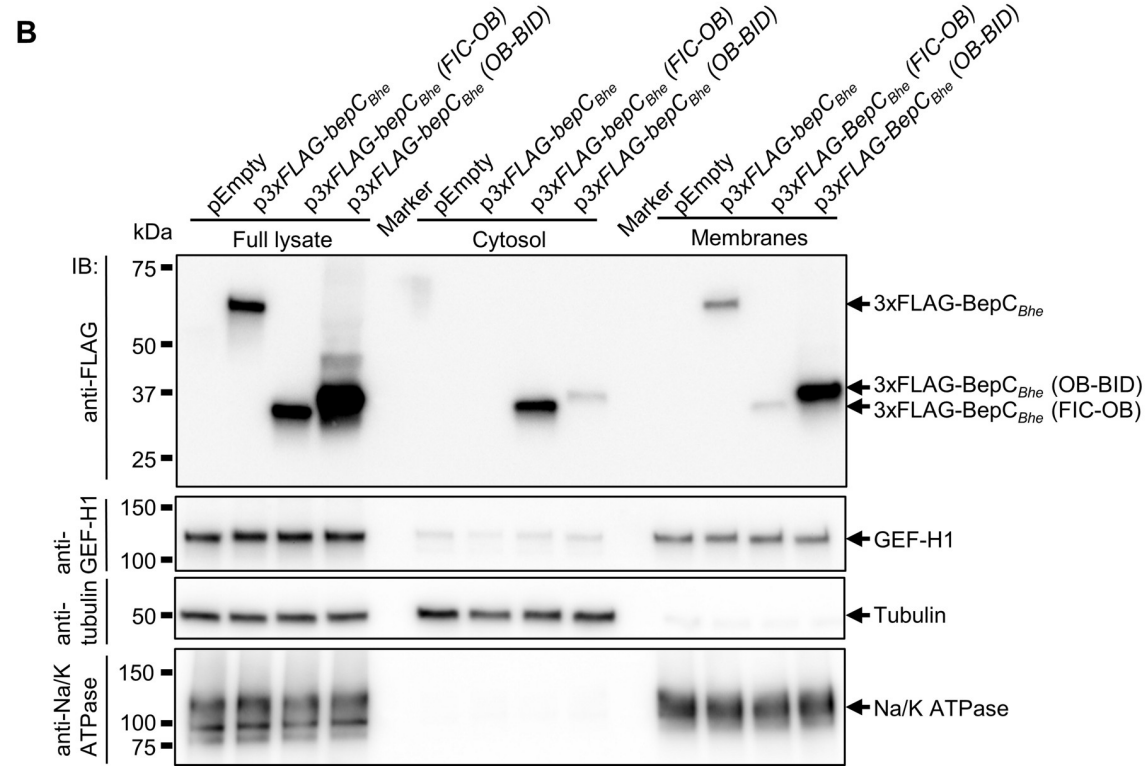
B
pEmpty
p3xFLAG-bepC$_{Bhe}$
p3xFLAG-bepC$_{Bhe}$ (FIC-OB)
p3xFLAG-bepC$_{Bhe}$ (OB-BID)
Marker
kDa
Full lysate
Cytosol
Membranes
IB:
anti-FLAG
anti-GEF-H1
anti-tubulin
anti-Na/K ATPase
3xFLAG-BepC$_{Bhe}$
3xFLAG-BepC$_{Bhe}$ (OB-BID)
3xFLAG-BepC$_{Bhe}$ (FIC-OB)
GEF-H1
Tubulin
Na/K ATPase

Fig 7. BepC$_{Bhe}$ recruits GEF-H1 to the plasma membrane via binding of the FIC-OB domain to GEF-H1 shown by pull-down and binding of the BID domain to the plasma membrane shown by subcellular fractionation. (**A**) HeLa cells were co-transfected with an expression plasmid for eGFP-GEF-H1 or eGFP and the indicated plasmids for expression of either 3xFLAG-BepC$_{Bhe}$, 3xFLAG-BepC$_{Bhe}$(FIC-OB), or 3xFLAG-BepC$_{Bhe}$(OB-BID). After 24 h, cell lysates were prepared and used for a FLAG pull-down assay. Bound proteins were analyzed by immunoblot with anti-FLAG, anti-GEF-H1 and anti-GFP antibodies. The signal visible in the anti-GFP blot for the marker lane was probably due to unspecific cross-reactivity. (**B**) HeLa cells were transfected with 3xFLAG-BepC$_{Bhe}$, 3xFLAG-BepC$_{Bhe}$(FIC-OB), or 3xFLAG-BepC$_{Bhe}$(OB-BID) for 24 h, then cell lysates were prepared, separated into membrane and cytosolic fractions and analyzed by immunoblot with anti-FLAG and anti-GEF-H1 antibodies. Anti-tubulin and anti-Na/K ATPase antibodies were used as cytosolic and membrane markers, respectively. Shown are representative results from three independent experiments.

https://doi.org/10.1371/journal.ppat.1008548.g007

deregulation of an endogenous GEF that would be beneficial for stealth pathogens involved in chronic infections. We show that the T4SS-translocated effector BepC of *Bartonella* spp. recruits GEF-H1 to the plasma membrane, thereby activating the RhoA/ROCK signaling pathway and leading to actin rearrangements.

While some bacterial effectors induce microtubule depolymerization to release GEF-H1 and eventually activate the RhoA pathway [39], VopO, a T3SS effector from *Vibrio parahaemolyticus*, is the only bacterial effector reported to interact directly with GEF-H1 and activate the RhoA pathway, thereby triggering actin stress fiber formation [2]. However, the mechanism of GEF-H1 activation by VopO remained elusive as co-localization studies did not show an alteration of GEF-H1 localization or an increase of its GEF activity.

Given that BepC contains a FIC domain, which in the context of other Fic proteins is known to catalyze posttranslational modifications [20,21,28], it was conceivable to assume that the BepC-triggered actin phenotype might be associated with a putative enzymatic activity. However, the mutation of four essential amino acids in the conserved FIC motif of BepC$_{Bhe}$ (H146A, K150A, R154A, R157A) or the exchange of the flap region required for registration of the target amino acid did not display any negative impact on actin stress fiber formation. Assuming that these modifications have compromised, if not fully eliminated a putative catalytic activity, we concluded that BepC acts likely on GEF-H1 via protein-protein interactions rather than by posttranslational modification. As the FIC motif is highly conserved between BepC homologs of different *Bartonella* species, it may still play another significant role during infection and we cannot exclude that BepC catalyzes a posttranslational modification on an unrelated target that is irrelevant for BepC-triggered actin stress fiber formation.

Interestingly, the unexpected finding that a FIC domain exerts a biological function unrelated to a catalytic activity is unique and only remotely reminiscent of the Fic protein AvrB, which lacks all residues required for enzymatic activity [40]. Thus, it opens new perspectives for the function of the many Beps, and other Fic proteins, carrying a non-canonical FIC motif and possibly also lacking enzymatic activity [16,20,41].

Corroborating evidences, obtained by fluorescent microscopy, pull-down experiments and subcellular fractionation analysis, of BepC$_{Bhe}$ full-length and its FIC-OB or OB-BID truncation constructs regarding their association with membranes and their interaction with GEF-H1, allowed us to develop a simple model of the activation of GEF-H1 by BepC$_{Bhe}$ (Fig 8). BepC$_{Bhe}$ full-length was found to localize to the plasma membrane and recruit GEF-H1 from its canonical microtubule-bound location. In sharp contrast, BepC$_{Bhe}$ (FIC-OB) was found in the cytoplasm fraction and co-localized with eGFP-GEF-H1 at microtubules, indicating that the soluble FIC domain binds to GEF-H1 without dissociating GEF-H1 from microtubules. On the contrary, OB-BID associated with the plasma membrane without any sign of co-localization with GEF-H1 and showed poor binding in pull-down assays. Consistent with the latter finding, the BID domain of BepC$_{Bhe}$ was previously reported to localize to the plasma membrane after ectopic expression in HEK293T cells [14]. Accordingly, ectopic expression of mCherry-tagged BepC$_{Bhe}$ full-length in HUVECs was also reported to localize to the plasma membrane [11]. In conclusion, BepC$_{Bhe}$ appears to bind GEF-H1 via the FIC domain and

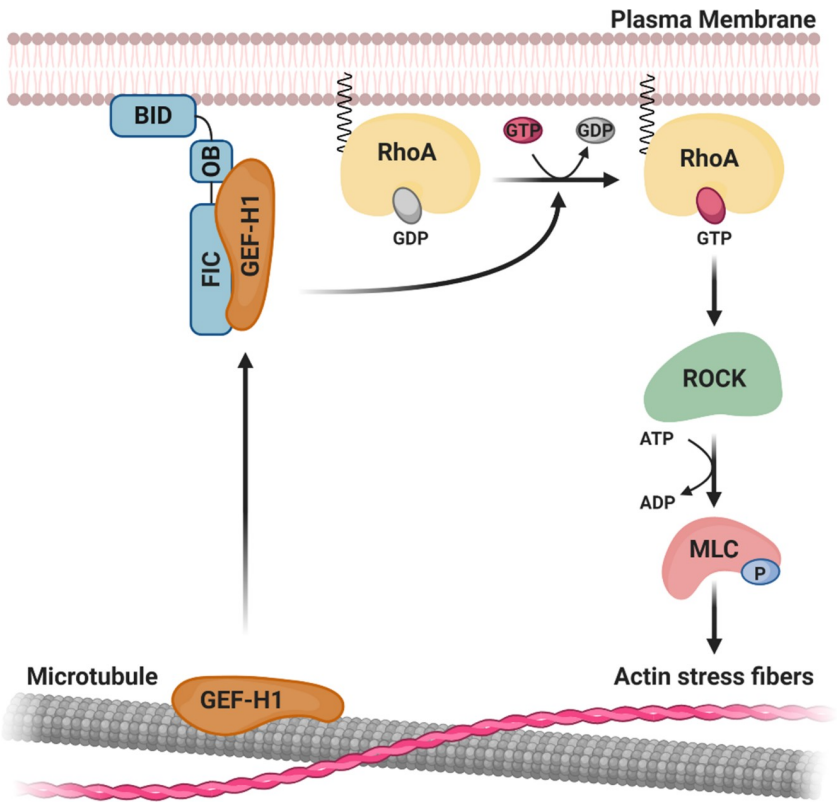

Fig 8. Model of BepC-triggered actin stress fibers formation mediated by the recruitment of GEF-H1 to the plasma membrane. Upon translocation, BepC localizes to the plasma membrane via its BID domain and binds GEF-H1 via its FIC-OB domains. There, GEF-H1 activates RhoA by exchanging GDP for GTP, allowing activation of the downstream kinase ROCK. ROCK-dependent phosphorylation of myosin light chain (MLC) will then induce actin stress fibers formation.

https://doi.org/10.1371/journal.ppat.1008548.g008

recruit it to the plasma membrane via anchorage by the BID domain (Fig 8). Although further investigation is required to determine how GEF-H1 is recruited from the microtubule-bound state, we can formulate two hypotheses: i) Either membrane-bound BepC recruits over time the GEF-H1 sub-pool that is cycling between microtubules and the plasma membrane in the course of other signaling processes, or ii) $BepC_{Bhe}$ full-length has the capacity to actively dissociate GEF-H1 from the microtubules and to relocalize it to the plasma membrane. In both cases, the GEF-H1 pool recruited to $BepC_{Bhe}$ at the plasma membrane should lead to activation of membrane-anchored RhoA via its GEF activity, followed by activation of the downstream Rho kinase ROCK, which in turn phosphorylates myosin light chain (MLC), eventually leading to actin stress fiber formation (Fig 8). Our data on Rho and ROCK inhibitors and phosphorylation of myosin light chain support an activation of this signaling cascade downstream of GEF-H1. Although the BepC-triggered F-actin phenotype is dominated by the prominent formation of stress fibers via the RhoA pathway, we cannot exclude that GEF-H1 also activates to some extend Rac1 as it has been shown in other physiological conditions [34], which may trigger additional F-actin changes such as cortical F-actin formation and membrane ruffling.

In conclusion, we characterized a novel molecular mechanism by which bacterial pathogens may selectively activate a Rho GTPase pathway via the recruitment of GEF-H1 to the plasma membrane.

Interestingly, BepC and GEF-H1 were found to be part of a bigger complex containing MRCKα, however, it remained unclear whether this kinase also interacts with BepC, or

whether it binds primarily via GEF-H1 or possibly additional proteins in this complex. Yet, we can conclude that the participation of MRCKα is neglectable for BepC-triggered cytoskeletal changes given that a full knock-out of MRCKα did not interfere with actin stress fiber formation mediated by the effector. Nevertheless, it is also conceivable that under relevant physiological conditions prone to activation of MRCKα, the interaction with GEF-H1 may contribute to BepC-triggered stress fiber formation via direct phosphorylation of MLC and inhibition of myosin light chain phosphatase (MLCP) [42] (see model in Fig 4B).

The high level of sequence conservation between BepC homologs [16] and the consistency in the ability to trigger actin rearrangements indicate an evolutionary conserved molecular function that is playing a major role in the context of a shared infection strategy of the bartonellae [6,7]. Thus, future work should place this effector signaling mechanism into a larger pathophysiological context of *Bartonella* spp. infection in the established infection models for invasome formation and alternative modes of bacterial internalization [12,24–26], migration of infected dendritic cells [11], and related innate immune cell functions [5,43].

Materials and methods

Bacterial strains and growth conditions

The bacterial strains used in this study are listed in S2 Table. *Bartonella* species were grown on Columbia blood agar (CBA, Oxoid, CM0331) plates containing 5% defibrinated sheep blood (Oxoid, SR0051) at 35˚C and 5% CO_2 for 3 days then expended for 2 days on new plates. When necessary, media were supplemented with 30 μg/ml kanamycin, 100 μg/ml streptomycin. *E. coli* strain was cultivated in Luria-Bertani liquid medium (LB) or on LB agar on plates (LA) at 37˚C overnight. Media were supplemented with 50 μg/ml kanamycin and 1 mM diaminopimelic acid (DAP, Sigma, D1377).

The *Bhe* Δ*bepA-G*, Δ*virB4* mutant was generated by a two-step gene replacement procedure as described previously [38]. In brief pRS25 [39] was used to generate an in-frame *ΔvirB4* deletion in the MSE150 *Bhe* Δ*bepA-G* background [8] resulting in the strain LU B2-61.

Construction of plasmids used in this work

Bartonella expression plasmids used in this study are listed in S3 Table. Eukaryotic expression plasmids used in this study are listed in S4 Table. Plasmids construction details as summarized in S5 Table and S6 Table and the used PCR primers as listed in S7 Table.

Conjugation of *Bartonella*-expression plasmids into *Bartonella*

Bartonella henselae Δ*bepA-G* (MSE150) was grown on CBA plates in presence of 100 μg/ml streptomycin at 35˚C and 5% CO_2 for 3 days then expanded on new plates for 2 days. The day before conjugation, 5 ml of LB containing 1 mM DAP and 50 μg/ml kanamycin were inoculated with a conjugation strain (JKE170) containing the plasmid of interest. After overnight incubation at 37˚C, a subculture was prepared by inoculating 5 ml of LB containing 1 mM DAP and 50 μg/ml kanamycin with 200 μl of overnight culture before being incubated for 2 h at 37˚C. In order to remove antibiotics, 500 μl of the subculture was centrifuged for 4 min at 2'000 x g and the bacterial pellet was resuspended in 500 μl of M199 (Gibco, 22340–020) supplemented with 10% of heat-inactivated fetal calf serum (FCS), the washing step was repeated once. The same process was applied to *Bartonella*, bacteria were harvested in 1 ml of M199 10% heat-inactivated FCS and centrifuged for 4 min at 2'000 x g. The bacterial pellet was resuspended in 500 μl of M199 10% heat-inactivated FCS before being centrifuged again and resuspended in 100 μl of M199 10% heat-inactivated FCS. 20 μl of *E. coli* were mixed with 100 μl of

Bartonella and incubated for 5 h at 35˚C, 5% CO_2 on a nitrocellulose filter deposited on a CBA plate supplemented with 1 mM of DAP. The filter was transferred in an Eppendorf tube containing 1 ml of M199 10% heat-inactivated FCS and the bacteria were resuspended by gently shaking. 50 μl were plated on a CBA plate supplemented with 30 μg/ml kanamycin and 100 μg/ml streptomycin. A single colony was selected and subsequently tested to confirm the presence of the plasmid.

Analysis of effector protein expression in *B. henselae*

B. henselae were grown on CBA plates for three days and expended for 2 days on new plates as described above. To analyze protein expression, bacteria were inoculated at OD 0.1 in 5 ml of M199 containing 10% heat-inactivated FCS with 10 μM IPTG and grown at 35˚C and 5% CO_2 for 24 h. Bacteria were harvested by centrifugation, the bacterial pellet was resuspended in SDS-sample buffer to obtain OD 1 and analyzed by immunoblot.

Cell culture

Human umbilical vein endothelial cells (HUVEC) were isolated as described before (Dehio et al., 1997) and cultured at 37˚C with 5% CO_2 in Endothelial Cell Growth Medium (ECGM, Promocell, C-22010) supplemented with Endothelial Cell Growth Medium SupplementMix (Promocell, C-39215).

HeLa cells were cultured at 37˚C with 5% CO_2 in DMEM (Sigma, D6429) supplemented with 10% heat-inactivated FCS.

Cell infection for microscopy

HUVECs were plated at a density of 3'000 cells/well in a 96-well plate (Corning, #3904) precoated with 0.2% of gelatin using supplemented ECGM. HeLa cells were seeded at a density of 12'500 cells/well in a μ-Slide 8 Well (Ibidi, Cat. N˚:80826) or at a density of 2'000 cells/well in a 96-well plate (Corning, #3904) using DMEM supplemented with 10% heat-inactivated FCS. The next day, cells were infected with *Bartonella* at the indicated MOI in M199 (Gibco, 22340–020) supplemented with 10% of heat-inactivated FCS in presence of 10 μM of isopropyl-β-D-thiogalactoside (IPTG, Biochemica, A1008). After incubation at 35˚C and 5% CO_2, cells were fixed with 3.7% of paraformaldehyde for 10 minutes and washed 3 times with PBS.

Cell transfection

HeLa cells were seeded at a density of 12'500 cells/well in a μ-Slide 8 Well (Ibidi, Cat. N˚:80826) or at a density of 2'000 cells/well on a 96-well plate (Corning, #3904) using DMEM supplemented with 10% of heat-inactivated FCS. The next day, cells were transfected according to manufacturer instruction with a transfection mix containing a ratio of 1 μg of plasmid for 2 μl FuGene HD transfection reagent (Promega, REF E2311) diluted in DMEM without FCS. After transfection for 24 h at 37˚C and 5% CO_2, cells were fixed with 3.7% of paraformaldehyde for 10 minutes and washed 3 times with PBS.

Immunostaining

Fixed cells were permeabilized for 10 minutes with PBS 0.2% BSA (Sigma, A9647) and 0.5% Triton X-100 (Sigma, T9284). After being washed 3 times with PBS with 0.2% BSA, cells were incubated overnight at 4˚C in the presence of the primary antibody (S8 Table) diluted in PBS with 0.2% BSA. After 2 more washes with PBS with 0.2% BSA, cells were incubated for 2 h in the dark in presence of the secondary antibody (S8 Table), DAPI (Sigma, D9542, 1 μg/ml) and,

when indicated, DY-547P1 phalloidin (Dyomics GmbH, final concentration 1/250) diluted in PBS with 0.2% BSA. Cells were finally washed 3 times with PBS. 96-well plates were imaged with an MD ImagXpress Micro automated microscope from Molecular devices and fluorescence was detected at 10x magnification. Images were processed in MetaXpress. For μ-Slide, the stained samples were analyzed using a LEICA point scanning confocal "SP8"microscope (Imaging Core Facility, Biozentrum, University of Basel, Switzerland). Z-stacks with 34–40 focal planes with a spacing of 0.45 μm were recorded and images were reconstructed by Z-projection using ImageJ.

Subcellular fractionation of cell lysates

Subcellular fractionation was based on procedures described before [40] with some modifications. In brief, cells were washed three times with cold PBS, before swelling buffer (50 mM Hepes pH 7.5, 15 mM NaCl, 2mM MgCl2, protease inhibitors) was added. Cells were harvested by scraping, transferred to a 1.5 ml tube and incubated 15 min on ice. Then cells were lysed by sonication (2x 10 pulses, 100% intensity) and incubated again for 15 min on ice. A sample of the resulting cell lysate was kept as full lysate. The remaining sample was fractionated by centrifugation. The nuclei fraction was separated by centrifugation at 800 x *g* for 15 min at 4˚C, the supernatant was further fractionated by centrifugation at 100,000 × *g* for 1 hour at 4˚C into the cytosolic supernatant fraction and the membrane pellet. For analysis by immunoblot, SDS-sample buffer was added. The membrane fraction was resuspended in swelling buffer containing 1% Nonidet P40 substitute (Sigma, 74385) before addition of the sample buffer. To facilitate solubilization, sample were twice heated at 95˚C and sonicated. Analysis was performed via immunoblot as described below.

Pull-down assay

HeLa cells or HUVECs were plated in round plates (Falcon, REF 353003) at a density of 365'000 or 544'000 cells per plate, respectively. The cells were then incubated overnight at 37˚C with 5% CO_2 in DMEM complemented with 10% heat-inactivated FCS. In the morning, cells have been infected with the indicated strain of *Bartonella* at MOI of 200 for 24 h at 35˚C with 5% CO_2 in M199 supplemented with 10% heat-inactivated FCS in presence of 10 μM of IPTG. After infection, cells were washed 3 times with ice-cold PBS and lysed with lysis buffer containing 50 mM Hepes (pH 7.5), 150 mM NaCl, protease inhibitor (Roche, 11836170001), and 1% Nonidet P40 substitute (Sigma, 74385). Cell lysates were collected with a cell scraper and incubated 30 minutes on ice. After centrifugation at 20'000 x g for 30 min at 4˚C, the supernatants were incubated in presence of 20 μl of protein G agarose beads (Roche, 11243233001) for 3 h at 4˚C on a rotor to reduce unspecific binding. After removing the beads by centrifugation for 30 seconds at 12'000 x g, 2 μg of antibody (S8 Table) was added to the supernatant. After 3 h of incubation at 4˚C on a rotor, 20 μl of protein G agarose was added to the lysates and incubated overnight at 4˚C on a rotor. The next morning, agarose beads were collected by centrifugation for 30 seconds at 12'000 x g before being washed 2 times with lysis buffer and 2 more times with lysis buffer without NP-40. Proteins were eluted from the beads by incubation at 95˚C for 10 minutes in SDS sample buffer. Elution fractions and cell lysates before pull-down were analyzed by immunoblot. The same protocol was applied for samples analyzed by mass spectrometry although one cell culture flask of 150 cm2 was used per infection and that proteins were eluted by incubation at 95˚C for 10 minutes with 2% SDS.

Sample preparation for mass spectrometry

Proteins were precipitated with trichloroacetic acid and incubated 10 min at 4˚C. The protein pellet was washed twice with cold acetone and resuspended with 4 M urea. Then the samples

were treated with 5 mM of tris(2-carboxyethyl)phosphine (TCEP) for 30 min at 37˚C in order to reduce disulfide bonds. After incubation, iodoacetamide (1.8 mg/ml final) was added to the samples to irreversibly prevent the formation of disulfide bonds and incubated for 30 min at 25˚C in the dark. The samples were subsequently diluted with 0.1 M ammonium bicarbonate to have a final concentration of urea of 1.6 M. For digestion, the proteins were incubated overnight at 37˚C in presence of 1 μg of trypsin. After acidification with trifluoroacetic acid (TFA, 1% final), the peptides were loaded on a C-18 column (The Nest Group, SS18V) pre-equilibrated with buffer A (0.1% TFA). The column was washed 3 times with buffer C (5% acetonitrile / 95%water (v/v) and 0.1% TFA) and peptides were eluted with buffer B (50% acetonitrile / 50%water (v/v) and 0.1% TFA). The peptides were finally dried under vacuum and kept at—80˚C. Before LC-MS/MS mass analysis, samples were resuspended in 0.1% formic acid by sonication.

Mass spectrometry analysis

For each sample, aliquots of 0.4 μg of total peptides were subjected to LC-MS analysis using a dual pressure LTQ-Orbitrap Elite mass spectrometer connected to an electrospray ion source (both Thermo Fisher Scientific) and a custom-made column heater set to 60˚C. Peptide separation was carried out using an EASY nLC-1000 system (Thermo Fisher Scientific) equipped with a RP-HPLC column (75μm × 30cm) packed in-house with C18 resin (ReproSil-Pur C18–AQ, 1.9 μm resin; Dr. Maisch GmbH, Germany) using a linear gradient from 95% solvent A (0.1% formic acid in water) and 5% solvent B (80% acetonitrile, 0.1% formic acid, in water) to 35% solvent B over 50 minutes to 50% solvent B over 10 minutes to 95% solvent B over 2 minutes and 95% solvent B over 18 minutes at a flow rate of 0.2 μl/min. The data acquisition mode was set to obtain one high resolution MS scan in the FT part of the mass spectrometer at a resolution of 120,000 full width at half maximum (at 400 m/z, MS1) followed by MS/MS (MS2) scans in the linear ion trap of the 20 most intense MS signals. The charged state screening modus was enabled to exclude unassigned and singly charged ions and the dynamic exclusion duration was set to 30 s. The collision energy was set to 35%, and one microscan was acquired for each spectrum.

Protein identification and label-free quantification

The acquired raw-files were imported into the Progenesis QI software (v2.0, Nonlinear Dynamics Limited), which was used to extract peptide precursor ion intensities across all samples applying the default parameters. The generated mgf files were searched using MASCOT against a decoy database containing normal and reverse sequences of the concatenated *Homo sapiens* (UniProt, Mai 2016) and *Bartonella henselae* (UniProt, July 2016) proteome and commonly observed contaminants (in total 44102 sequences) generated using the SequenceReverser tool from the MaxQuant software (Version 1.0.13.13). The following search criteria were used: full tryptic specificity was required (cleavage after lysine or arginine residues, unless followed by proline); 3 missed cleavages were allowed; carbamidomethylation (C) was set as fixed modification; oxidation (M) and protein N-terminal acetylation were applied as variable modifications; mass tolerance of 10 ppm (precursor) and 0.6 Da (fragments) was set. The database search results were filtered using the ion score to set the false discovery rate (FDR) to 1% on the peptide and protein level, respectively, based on the number of reverse protein sequence hits in the datasets. Quantitative analysis results from label-free quantification were normalized and statically analyzed using the SafeQuant R package v.2.3.4 (https://github.com/eahrne/SafeQuant/) (PMID: 27345528) to obtain protein relative abundances. This analysis included summation of peak areas per protein and LC MS/MS run followed by calculation of protein

abundance ratios. Only isoform specific peptide ion signals were considered for quantification. The summarized protein expression values were used for statistical testing of differentially abundant proteins between conditions. Here, empirical Bayes moderated t-Tests were applied, as implemented in the R/Bioconductor limma package (http://bioconductor.org/packages/release/bioc/html/limma.html). The resulting p-values were adjusted for multiple testing using the Benjamini Hochberg method.

All LC-MS analysis runs are acquired from independent biological samples. To meet additional assumptions (normality and homoscedasticity) underlying the use of linear regression models and Student t-Test MS-intensity signals are transformed from the linear to the log-scale.

Unless stated otherwise linear regression was performed using the ordinary least square (OLS) method as implemented in base package of R v.3.1.2 (http://www.R-project.org/). The sample size of three biological replicates was chosen assuming a within-group MS-signal Coefficient of Variation of 10%. When applying a two-sample, two-sided Student's t-test this gives adequate power (80%) to detect protein abundance fold changes higher than 1.65, per statistical test. Note that the statistical package used to assess protein abundance changes, SafeQuant, employs a moderated t-Test, which has been shown to provide higher power than the Student's t-test. We did not do any simulations to assess power, upon correction for multiple testing (Benjamini-Hochberg correction), as a function of different effect sizes and assumed proportions of differentially abundant proteins.

Inhibitor treatment of infected HeLa cells

HeLa cells were seeded at a density of 2'000 cells/well on a 96-well plate (Corning, #3904) using DMEM supplemented with 10% of heat-inactivated FCS. After overnight incubation at 37˚C with 5% CO_2, cells were infected with *Bhe* Δ*bepA-G* carrying the empty plasmid or expressing BepC at MOI of 400 in M199 (Gibco, 22340–020) supplemented with 10% of heat-inactivated FCS in presence of 10 μM of IPTG. After 24 h of incubation at 35˚C and 5% CO_2, the medium was removed and cells were incubated with inhibitor diluted in DMEM at 35˚C with 5% CO_2. The treatment consisted of Rho inhibitor I (Cytoskeleton, CT04) for 2 h or Y27632 (Sigma, Y0503) for 1 hour at the indicated concentration. The experiment was stopped by fixation with 3.7% of paraformaldehyde for 10 minutes. Finally, the cells were washed 3 times with PBS before being stained and imaged by microscopy.

Generation of knock-out cells

HeLa cells were seeded at a density of 1'400'000 cells per 150 cm2 flask in DMEM supplemented with 10% of heat-inactivated FCS and incubated overnight at 37˚C with 5% CO_2. The day after, in 1.2 ml of DMEM without FCS, 12 μg of plasmid encoding GFP and the guide RNA (gRNA) targeting the first exon of the gene of interest were mixed with 12 μg of plasmid carrying the puromycin resistance gene and the gRNA targeting the last exon. After adding 48 μl of FuGene HD transfection reagent (Promega, E2311), the transfection mix was incubated for 15 min at room temperature before being transferred in the cell culture flask. The cells were transfected for 24 h at 37˚C with 5% CO_2. Double-transfected cells were selected in the presence of puromycin (1.5 μg/ml) for 24 h at 37˚C with 5% CO_2 followed by FACS to select GFP-positive cells. Selected cells were collected in DMEM with 10% heat-inactivated FCS supplemented with penicillin-streptomycin and expanded for several days. Finally, cells were stored at -80˚C in DMEM supplemented with 10% heat-inactivated FCS and 10% DMSO. The expression level of the protein of interest was monitored via immunoblot.

Immunoblot analysis

The samples used for immunoblot analysis were separated by SDS-PAGE on a 4–20% gradient gel (Mini-PROTEAN TGX Gels, Biorad, Cat# 456–1093). Gel electrophoresis was performed at 120 V in running buffer (Tris-glycine, 0.1% SDS). Proteins were transferred on a PVDF membrane (GE Healthcare, 10600021) via wet electroblotting at 100 V in transfer buffer (20% methanol, Tris-glycine) at 4˚C. After transfer, the membrane was incubated for 1 hour in blocking buffer (PBS, 0.1% Tween 20 (Sigma, 93773), supplemented with 5% milk or 5% BSA according to antibody recommendation). After washing with PBS 0.1% Tween 20, the membrane was incubated overnight at 4˚C in blocking buffer with the primary antibody (S8 Table). The membrane was washed again with PBS 0.1% Tween 20 before being incubated 1 hour at room temperature in blocking buffer with the secondary antibody (S8 Table). The blots were developed using LumiGLO Reserve Chemiluminescent Substrate System (KPL, 54-70-00, 54-69-00). Finally, the signal was detected with LAS4000 (Fujifilm).

Quantification of F-actin and pMLC via Cellprofiler

Experiments performed in 96-well plates were subjected to automated microscopy, using MD ImageXpress Micro automated microscopes. For each condition, at least 6 wells with 25 sites were imaged in 4 different wavelengths corresponding to the applied cell staining (DAPI, DY-547P1 phalloidin, pMLC, *Bartonella*). Images were analyzed with the CellProfiler software [41]. Two separate Cellprofiler pipelines are used for each assay. The first pipeline calculates a shading model, which is used by the second pipeline to correct images prior to analysis. To correct uneven illumination inherent in wide-field microscopic imaging (shading), an illumination function was computed. The illumination function was calculated on all images based on the Background method. The resulting image was smoothed using a Gaussian method with a 100-filter size. To reduce the signal originating from the bacterial DNA in the DAPI channel, the signal corresponding to *Bartonella* was subtracted from the DAPI image. On all images, CellProfiler was executed to perform object segmentation and measurements with the following steps. Nuclei were detected as primary objects using an Automatic strategy and clumped objects were identified based on their shape and segmented based on their intensity. HeLa cells were detected as secondary objects via their DY-547P1 phalloidin signal by using a Propagation method from the nuclei followed by a Global threshold strategy combined with an Otsu threshold method. The average of the mean intensity of each cell within one site was measured for the F-actin or pMLC signals. Data from all sites from the same conditions were compiled together. The mean cell intensity per site was normalized on the uninfected condition.

Statistical analysis

Graph was generated with GraphPad Prism 8. When data were not following a normal Gaussian distribution, statistical analyses were performed using Kruskal-Wallis test with Dunn's multiple comparison test. For the graph presented in the figures, significance was denoted as ajusted P-value $P^{*} < 0.1$, $P^{**} < 0.01$, $P^{***} < 0.001$, $P^{****} < 0.0001$.

Software

ImageJ [42] was used to create z-projection and x-z sections of confocal microscopy images. MetaXpress (Molecular Devices) was used to acquire and generate microscopy pictures from automated microscope. Image analysis and the calculation of the average of the mean cell fluorescence intensity was realized via Cellprofiler [41]. GraphPad prism 8 (GraphPad) was used

to create the dot-plot and the statistical analysis. Geneious Prime 2019 (Geneious) was used to design cloning of plasmids. The schematic model of BepC-mediated actin stress fiber formation was created with Biorender.com.

Supporting information

S1 Fig. BepC$_{Bhe}$-triggered actin stress fiber formation in *B. henselae*-infected HUVECs is dependent on time and multiplicity of infection. (**A, B**) HUVECs were infected with isogenic *Bhe* Δ*bepA-G* strains expressing 3xFLAG-tagged BepC$_{Bhe}$ wild-type or mutant versions or carrying the empty plasmid at indicated MOIs for 24 or 48 h. After fixation, cells were stained by immunocytochemistry, followed by fluorescence microscopy analysis. (**A**) Shown are representative images for *Bhe* Δ*bepA-G* strains expressing 3xFLAG-tagged BepC$_{Bhe}$ wild-type and the isogenic empty plasmid control. F-actin is represented in green, DNA in blue, and bacteria in red (scale bar = 50 μm). (**B**) The graphs show the relative mean fluorescence intensity of the F-actin signal at 24 hpi (left panel) and 48h (right panel) for the indicated MOIs normalized to the uninfected control. Shown are results from three independent experiments. BepC$_{Bhe}^{****}$ = BepC$_{Bhe}$ H146A, K150A, R154A, R157A; BepC$_{Bhe}$ (Flap BepA$_{Bhe}$) = BepC$_{Bhe}$ A90E, R92K, P93R, K94T, H96W, R97K, V98N, P99A; BepC$_{Bhe}$ (OB-BID) = BepC$_{Bhe}$ Δ1–226.
(PDF)

S2 Fig. Expression of 3xFLAG-tagged BepC$_{Bhe}$ in infected and transfected HeLa cells. (**A**) HeLa cells were infected with isogenic *Bhe* Δ*bepA-G* strains expressing FLAG-tagged BepC$_{Bhe}$ wild-type or mutant versions or carrying the empty plasmid at multiplicity of infection (MOI) of 400. After 48 h of infection, cells were fixed and immunocytochemically stained with anti-FLAG antibody, followed by fluorescence microscopy analysis. FLAG staining is shown in white and corresponds to the images displayed in Fig 2A (scale bar = 50 μm). (**B**) HeLa cells were transfected with indicated plasmids for expression of FLAG-tagged BepC$_{Bhe}$ wild-type, mutant versions, or truncations, or no protein as negative control (pEmpty). 24 h after transfection, cells were fixed and immunocytochemically stained, followed by fluorescence microscopic analysis. FLAG staining is represented in white and corresponds to the images displayed in Fig 3B (scale bar = 50 μm). BepC$_{Bhe}^{****}$ = BepC$_{Bhe}$ H146A, K150A, R154A, R157A. Shown are representative results of three independent experiments.
(PDF)

S3 Fig. The BepC$_{Bhe}$-triggered actin stress fiber formation phenotype in *B. henselae*-infected HeLa cells is type-IV-secretion-dependent. (**A**) HeLa were infected with *Bhe* Δ*bepA-G or Bhe* Δ*bepA-G*, Δ*virB4* expressing 3xFLAG-tagged BepC$_{Bhe}$ or carrying empty plasmid as a negative control at MOI 400 for 48 h. After fixation, cells were stained by immunocytochemistry, followed by fluorescence microscopy analysis. F-actin is represented in green, DNA in blue, and bacteria in red (scale bar = 50 μm). (**B**) Expression of 3xFLAG-tagged BepC$_{Bhe}$ in *Bhe* Δ*bepA-G* and *Bhe* Δ*bepA-G*, Δ*virB4* was analyzed by immunoblot using an anti-FLAG antibody. (**C**) The mean fluorescence intensity of F-actin shown for conditions shown in (A) were quantified for each individual cell using CellProfiler. Data are represented as dot plots with each data point corresponding to the average of all mean cell intensity values within one imaged site normalized to the uninfected control. Statistical significance was determined using Kruskal-Wallis test (**** corresponds to p-value $\leq$ 0.0001). (**D**) Corresponding FLAG channel of conditions shown in (A). FLAG staining is represented in white (scale bar = 50 μm). Data show a representative example of three independent experiments.
(PDF)

S4 Fig. BepC-triggered actin stress fiber formation is conserved among homologs encoded by various *Bartonella* species. (A) HeLa cells were infected with the indicated isogenic *Bhe* Δ*bepA-G* strains expressing FLAG-tagged BepC homologs at MOI of 400. After 48 h cells were fixed and immunocytochemically stained, followed by fluorescence microscopy analysis. F-actin is represented in green, DNA in blue, and bacteria in red (scale bar = 50 μm). (**B**) Expression of FLAG-tagged BepC homologues in *Bhe* Δ*bepA-G* was analysed in bacterial lysates by immunoblot analysis with an anti-FLAG antibody. (**C**) The mean fluorescence intensity of F-actin shown for conditions shown in (A) was quantified for each individual cell using CellProfiler. Data are represented as dot plots with each data point corresponding to the average of all mean cell intensity values within one imaged site. Statistical significance was determined using Kruskal-Wallis test (**** corresponds to p-value $\leq$ 0.0001). (**D**) HeLa cells were transfected for 24h with indicated expression plasmids encoding different BepC homologs. Cells were fixed and immunocytochemically stained, followed by fluorescence microscopy analysis. F-actin is represented in green and DNA in blue (scale bar = 50 μm). (**E**) Expression of FLAG-tagged BepC homologues was analysed in cellular lysates by immunoblot with an anti-FLAG antibody. (**F**) The mean fluorescence intensity of F-actin shown for conditions shown in (D) was quantified for each individual cell using CellProfiler. Data are represented as dot plots with each data point corresponding to the average of all mean cell intensity values within one imaged site. Statistical significance was determined using Kruskal-Wallis test (**** corresponds to p-value $\leq$ 0.0001). Data show a representative example of three independent experiments. *Bhe* (*B. henselae*); *Bqu* (*B. quintana*); *Btr* (*B. tribocorum*); *Bta* (*B. taylorii*); *Bgr* (*B. grahamii*).
(PDF)

S5 Fig. Inhibition of RhoA/B/C or ROCK reduces actin stress fiber formation mediated by $BepC_{Bhe}$. (**A**) Proposed model of BepC-triggered actin stress fiber formation via the activation of the RhoA pathway and the targets of inhibitors used for validation. (**B-E**) HeLa cells were infected at MOI of 400 with *Bhe* Δ*bepA-G* expressing 3xFLAG-tagged $BepC_{Bhe}$ or carrying the empty plasmid as a negative control for 24 h. Then cells were treated with inhibitors as specified below, followed by fixation and immunocytochemical staining. Specimen were then analyzed by fluorescence microscopy. F-actin is represented in white (scale bar = 50 μm). (**B**) Representative images of HeLa cells incubated for 2 h in the absence or presence of Rho inhibitor I at the indicated concentrations. (**C**) The mean fluorescence intensity of F-actin shown for conditions shown in (B) was quantified for each individual cell using CellProfiler. The graphs show the relative mean fluorescence intensity of the F-actin signal for the indicated condition normalized to the non-treated uninfected control. (**D**) Representative images of HeLa cells incubated for 1 h in the absence or presence of the ROCK inhibitor Y27632 at the indicated concentrations. (**E**) The mean fluorescence intensity of F-actin shown for conditions shown in (D) was quantified for each individual cell using CellProfiler. The graphs show the relative mean fluorescence intensity of the F-actin signal for the indicated condition normalized to the non-treated uninfected control. Data shown are representative results for three independent experiments.
(PDF)

S6 Fig. $BepC_{Bhe}$ induces a robust increase of myosin light chain phosphorylation. (**A**) Proposed model of BepC-triggered actin stress fiber formation. (**B**) HeLa cells were infected with isogenic *Bhe* Δ*bepA-G* strains expressing FLAG-tagged $BepC_{Bhe}$ wild-type or mutant variants, or carrying the empty plasmid at multiplicity of infection (MOI) of 200. After 48 h of infection, cells were fixed and immunocytochemically stained, followed by fluorescence microscopy analysis. Phosphorylated myosin light chain (pMLC) is represented in white (scale

bar = 50 μm). $BepC_{Bhe}^{****}$ = $BepC_{Bhe}$ H146A, K150A, R154A, R157A. (**C**) The mean fluorescence intensity of F-actin shown for conditions shown in (B) was quantified for each individual cell using CellProfiler. Data are represented as dot plots with each data point corresponding to the average of all mean cell intensity values within one imaged site. Statistical significance was determined using Kruskal-Wallis test (**** corresponds to p-value $\leq$ 0.0001).
(PDF)

S1 Table. List of proteins identified by Mass spectrometry.
(XLSX)

S2 Table. List of bacterial strains used in this study.
(PDF)

S3 Table. List of *Bartonella* expression vectors used in this work.
(PDF)

S4 Table. List of eukaryotic expression plasmids used in this work.
(PDF)

S5 Table. Construction details for plasmids used in this work.
(PDF)

S6 Table. Construction details for CRISPR/Cas expression constructs used in this study.
(PDF)

S7 Table. List of primers used in this work.
(PDF)

S8 Table. List of antibodies used in this work.
(PDF)

Acknowledgments

We thank Drs. Maxime Québatte and Isabel Sorg for critically reading of the manuscript and helpful comments, and we are very grateful to Dr. Isabel Sorg for her support in manuscript revision and final editing. We thank Sarah Stiegeler and Drs. Raquel Conde-Alvarez, Simone Eicher and Kathrin Pieles for sharing initial findings on the BepC phenotype and BepC/GEF-H1 interaction, and Drs. Maxime Québatte and Alexander Harms for sharing a *Bartonella* expression vector. We thank the Proteomics Core Facility for performing mass spectrometry analyses, the FACS Core Facility for cell sorting, and the Imaging Core Facility for providing technical support. We also thank Prof. Perihan Nalbant (University of Duisburg-Essen, Germany) for providing the eGFP-GEF-H1 mammalian expression vector. The plasmids used to generate CRISPR/Cas knock-out cell lines, pSpCas9(BB)-2A-GFP (PX458) (Addgene plasmid # 48138; http://n2t.net/addgene:48138; RRID:Addgene_48138) and pSpCas9(BB)-2A-Puro (PX459) (Addgene plasmid # 48139; http://n2t.net/addgene:48139; RRID:Addgene_48139), were a gift from Feng Zhang. The Bruderholzspital Basel is acknowledged for providing human umbilical cords.

Author Contributions

Conceptualization: Christoph Dehio.

Data curation: Simon Marlaire.

Formal analysis: Simon Marlaire.

Funding acquisition: Christoph Dehio.

Investigation: Simon Marlaire.

Methodology: Simon Marlaire.

Project administration: Christoph Dehio.

Resources: Christoph Dehio.

Software: Simon Marlaire.

Supervision: Christoph Dehio.

Validation: Simon Marlaire.

Visualization: Simon Marlaire.

Writing – original draft: Simon Marlaire.

Writing – review & editing: Simon Marlaire, Christoph Dehio.

References

1. Aktories K. Rho-modifying bacterial protein toxins. Pathog Dis. 2015; 73(9):ftv091. Epub 2015/10/11. https://doi.org/10.1093/femspd/ftv091 PMID: 26454272.
2. Hiyoshi H, Okada R, Matsuda S, Gotoh K, Akeda Y, Iida T, et al. Interaction between the type III effector VopO and GEF-H1 activates the RhoA-ROCK pathway. PLoS Pathog. 2015; 11(3):e1004694. https://doi.org/10.1371/journal.ppat.1004694 PMID: 25738744; PubMed Central PMCID: PMC4349864.
3. Aktories K. Bacterial protein toxins that modify host regulatory GTPases. Nat Rev Microbiol. 2011; 9 (7):487–98. Epub 2011/06/17. https://doi.org/10.1038/nrmicro2592 PMID: 21677684.
4. Christie PJ. The Rich Tapestry of Bacterial Protein Translocation Systems. Protein J. 2019; 38(4):389–408. Epub 2019/08/14. https://doi.org/10.1007/s10930-019-09862-3 PMID: 31407127; PubMed Central PMCID: PMC6826261.
5. Sorg I, Schmutz C, Lu YY, Fromm K, Siewert LK, Bogli A, et al. A *Bartonella* Effector Acts as Signaling Hub for Intrinsic STAT3 Activation to Trigger Anti-inflammatory Responses. Cell Host Microbe. 2020; 27(3):476–85 e7. Epub 2020/02/27. https://doi.org/10.1016/j.chom.2020.01.015 PMID: 32101706.
6. Harms A, Dehio C. Intruders below the radar: molecular pathogenesis of *Bartonella* spp. Clin Microbiol Rev. 2012; 25(1):42–78. Epub 2012/01/11. https://doi.org/10.1128/CMR.05009-11 PMID: 22232371; PubMed Central PMCID: PMC3255967.
7. Wagner A, Dehio C. Role of distinct type-IV-secretion systems and secreted effector sets in host adaptation by pathogenic *Bartonella* species. Cell Microbiol. 2019; 21(3):e13004. Epub 2019/01/16. https://doi.org/10.1111/cmi.13004 PMID: 30644157; PubMed Central PMCID: PMC6519360.
8. Schulein R, Guye P, Rhomberg TA, Schmid MC, Schroder G, Vergunst AC, et al. A bipartite signal mediates the transfer of type IV secretion substrates of *Bartonella henselae* into human cells. Proc Natl Acad Sci U S A. 2005; 102(3):856–61. Epub 2005/01/12. https://doi.org/10.1073/pnas.0406796102 PMID: 15642951; PubMed Central PMCID: PMC545523.
9. Wagner A, Tittes C, Dehio C. Versatility of the BID domain: Conserved function as type-IV-secretion-signal and secondarily evolved effector functions within *Bartonella*-infected host cells. Front Microbiol. 2019; 10:921. Epub 2019/05/28. https://doi.org/10.3389/fmicb.2019.00921 PMID: 31130928; PubMed Central PMCID: PMC6509941.
10. Stanger FV, de Beer TAP, Dranow DM, Schirmer T, Phan I, Dehio C. The BID Domain of Type IV Secretion Substrates Forms a Conserved Four-Helix Bundle Topped with a Hook. Structure. 2017; 25 (1):203–11. Epub 2016/11/28. https://doi.org/10.1016/j.str.2016.10.010 PMID: 27889208; PubMed Central PMCID: PMC6121808.
11. Okujava R, Guye P, Lu YY, Mistl C, Polus F, Vayssier-Taussat M, et al. A translocated effector required for *Bartonella* dissemination from derma to blood safeguards migratory host cells from damage by co-translocated effectors. PLoS Pathog. 2014; 10(6):e1004187. Epub 2014/06/20. https://doi.org/10.1371/journal.ppat.1004187 PMID: 24945914; PubMed Central PMCID: PMC4063953.
12. Truttmann MC, Guye P, Dehio C. BID-F1 and BID-F2 domains of *Bartonella henselae* effector protein BepF trigger together with BepC the formation of invasome structures. PLoS One. 2011; 6(10):e25106. Epub 2011/11/02. https://doi.org/10.1371/journal.pone.0025106 PMID: 22043280; PubMed Central PMCID: PMC3197191.

13. Rhomberg TA, Truttmann MC, Guye P, Ellner Y, Dehio C. A translocated protein of *Bartonella henselae* interferes with endocytic uptake of individual bacteria and triggers uptake of large bacterial aggregates via the invasome. Cell Microbiol. 2009; 11(6):927–45. https://doi.org/10.1111/j.1462-5822.2009.01302.x PMID: 19302579.

14. Pulliainen AT, Pieles K, Brand CS, Hauert B, Bohm A, Quebatte M, et al. Bacterial effector binds host cell adenylyl cyclase to potentiate Galphas-dependent cAMP production. Proc Natl Acad Sci U S A. 2012; 109(24):9581–6. https://doi.org/10.1073/pnas.1117651109 PMID: 22635269; PubMed Central PMCID: PMC3386119.

15. Wang C, Fu J, Wang M, Cai Y, Hua X, Du Y, et al. Bartonella quintana type IV secretion effector BepE-induced selective autophagy by conjugation with K63 polyubiquitin chain. Cell Microbiol. 2019; 21(4): e12984. Epub 2018/11/22. https://doi.org/10.1111/cmi.12984 PMID: 30463105.

16. Harms A, Segers FH, Quebatte M, Mistl C, Manfredi P, Korner J, et al. Evolutionary Dynamics of Pathoadaptation Revealed by Three Independent Acquisitions of the VirB/D4 Type IV Secretion System in *Bartonella*. Genome Biol Evol. 2017; 9(3):761–76. Epub 2017/03/25. https://doi.org/10.1093/gbe/evx042 PMID: 28338931; PubMed Central PMCID: PMC5381568.

17. Engel P, Salzburger W, Liesch M, Chang CC, Maruyama S, Lanz C, et al. Parallel evolution of a type IV secretion system in radiating lineages of the host-restricted bacterial pathogen *Bartonella*. PLoS Genet. 2011; 7(2):e1001296. https://doi.org/10.1371/journal.pgen.1001296 PMID: 21347280; PubMed Central PMCID: PMC3037411.

18. Selbach M, Paul FE, Brandt S, Guye P, Daumke O, Backert S, et al. Host cell interactome of tyrosine-phosphorylated bacterial proteins. Cell Host Microbe. 2009; 5(4):397–403. Epub 2009/04/22. https://doi.org/10.1016/j.chom.2009.03.004 PMID: 19380118.

19. Siamer S, Dehio C. New insights into the role of Bartonella effector proteins in pathogenesis. Curr Opin Microbiol. 2015; 23:80–5. Epub 2014/12/03. https://doi.org/10.1016/j.mib.2014.11.007 PMID: 25461577.

20. Harms A, Stanger FV, Dehio C. Biological Diversity and Molecular Plasticity of FIC Domain Proteins. Annu Rev Microbiol. 2016; 70:341–60. Epub 2016/08/03. https://doi.org/10.1146/annurev-micro-102215-095245 PMID: 27482742.

21. Roy CR, Cherfils J. Structure and function of Fic proteins. Nat Rev Microbiol. 2015; 13(10):631–40. Epub 2015/08/25. https://doi.org/10.1038/nrmicro3520 PMID: 26299785.

22. Xiao J, Worby CA, Mattoo S, Sankaran B, Dixon JE. Structural basis of Fic-mediated adenylylation. Nat Struct Mol Biol. 2010; 17(8):1004–10. Epub 2010/07/14. https://doi.org/10.1038/nsmb.1867 PMID: 20622875; PubMed Central PMCID: PMC2920259.

23. Palanivelu DV, Goepfert A, Meury M, Guye P, Dehio C, Schirmer T. Fic domain-catalyzed adenylylation: insight provided by the structural analysis of the type IV secretion system effector BepA. Protein Sci. 2011; 20(3):492–9. https://doi.org/10.1002/pro.581 PMID: 21213248; PubMed Central PMCID: PMC3064829.

24. Dehio C, Meyer M, Berger J, Schwarz H, Lanz C. Interaction of *Bartonella henselae* with endothelial cells results in bacterial aggregation on the cell surface and the subsequent engulfment and internalisation of the bacterial aggregate by a unique structure, the invasome. J Cell Sci. 1997; 110 (Pt 18):2141–54. PMID: 9378764.

25. Truttmann MC, Rhomberg TA, Dehio C. Combined action of the type IV secretion effector proteins BepC and BepF promotes invasome formation of *Bartonella henselae* on endothelial and epithelial cells. Cell Microbiol. 2011; 13(2):284–99. Epub 2010/10/23. https://doi.org/10.1111/j.1462-5822.2010.01535.x PMID: 20964799.

26. Eicher SC, Dehio C. Bartonella entry mechanisms into mammalian host cells. Cell Microbiol. 2012; 14 (8):1166–73. Epub 2012/04/24. https://doi.org/10.1111/j.1462-5822.2012.01806.x PMID: 22519749.

27. Engel P, Goepfert A, Stanger FV, Harms A, Schmidt A, Schirmer T, et al. Adenylylation control by intra- or intermolecular active-site obstruction in Fic proteins. Nature. 2012; 482(7383):107–10. Epub 2012/01/24. https://doi.org/10.1038/nature10729 PMID: 22266942.

28. Garcia-Pino A, Zenkin N, Loris R. The many faces of Fic: structural and functional aspects of Fic enzymes. Trends Biochem Sci. 2014; 39(3):121–9. Epub 2014/02/11. https://doi.org/10.1016/j.tibs.2014.01.001 PMID: 24507752.

29. Lee IC, Leung T, Tan I. Adaptor protein LRAP25 mediates myotonic dystrophy kinase-related Cdc42-binding kinase (MRCK) regulation of LIMK1 protein in lamellipodial F-actin dynamics. J Biol Chem. 2014; 289(39):26989–7003. https://doi.org/10.1074/jbc.M114.588079 PMID: 25107909; PubMed Central PMCID: PMC4175338.

30. Tan I, Ng CH, Lim L, Leung T. Phosphorylation of a novel myosin binding subunit of protein phosphatase 1 reveals a conserved mechanism in the regulation of actin cytoskeleton. J Biol Chem. 2001; 276 (24):21209–16. Epub 2001/06/16. https://doi.org/10.1074/jbc.M102615200 PMID: 11399775.

31. Leung T, Chen XQ, Tan I, Manser E, Lim L. Myotonic dystrophy kinase-related Cdc42-binding kinase acts as a Cdc42 effector in promoting cytoskeletal reorganization. Mol Cell Biol. 1998; 18(1):130–40. https://doi.org/10.1128/mcb.18.1.130 PMID: 9418861; PubMed Central PMCID: PMC121465.

32. Krendel M, Zenke FT, Bokoch GM. Nucleotide exchange factor GEF-H1 mediates cross-talk between microtubules and the actin cytoskeleton. Nat Cell Biol. 2002; 4(4):294–301. https://doi.org/10.1038/ncb773 PMID: 11912491.

33. Meiri D, Marshall CB, Greeve MA, Kim B, Balan M, Suarez F, et al. Mechanistic insight into the microtubule and actin cytoskeleton coupling through dynein-dependent RhoGEF inhibition. Mol Cell. 2012; 45 (5):642–55. Epub 2012/03/13. https://doi.org/10.1016/j.molcel.2012.01.027 PMID: 22405273.

34. Birkenfeld J, Nalbant P, Yoon SH, Bokoch GM. Cellular functions of GEF-H1, a microtubule-regulated Rho-GEF: is altered GEF-H1 activity a crucial determinant of disease pathogenesis? Trends Cell Biol. 2008; 18(5):210–9. https://doi.org/10.1016/j.tcb.2008.02.006 PMID: 18394899.

35. Nobes CD, Hall A. Rho, rac, and cdc42 GTPases regulate the assembly of multimolecular focal complexes associated with actin stress fibers, lamellipodia, and filopodia. Cell. 1995; 81(1):53–62. Epub 1995/04/07. https://doi.org/10.1016/0092-8674(95)90370-4 PMID: 7536630.

36. Kim WY, Gonsiorek EA, Barnhart C, Davare MA, Engebose AJ, Lauridsen H, et al. Statins decrease dendritic arborization in rat sympathetic neurons by blocking RhoA activation. J Neurochem. 2009; 108 (4):1057–71. Epub 2009/02/12. https://doi.org/10.1111/j.1471-4159.2008.05854.x PMID: 19209406; PubMed Central PMCID: PMC4277848.

37. Uehata M. Y-27632. Selective probe of ROCK/Rho-kinase. Jikken Igaku. 1999; 17(7):850–5.

38. Schulein R, Dehio C. The VirB/VirD4 type IV secretion system of *Bartonella* is essential for establishing intraerythrocytic infection. Mol Microbiol. 2002; 46(4):1053–67. Epub 2002/11/08. https://doi.org/10.1046/j.1365-2958.2002.03208.x PMID: 12421311.

39. Schmid MC, Schulein R, Dehio M, Denecker G, Carena I, Dehio C. The VirB type IV secretion system of *Bartonella henselae* mediates invasion, proinflammatory activation and antiapoptotic protection of endothelial cells. Mol Microbiol. 2004; 52(1):81–92. Epub 2004/03/31. https://doi.org/10.1111/j.1365-2958.2003.03964.x PMID: 15049812.

40. Sorg I, Goehring UM, Aktories K, Schmidt G. Recombinant *Yersinia* YopT leads to uncoupling of RhoA-effector interaction. Infect Immun. 2001; 69(12):7535–43. Epub 2001/11/14. https://doi.org/10.1128/IAI.69.12.7535-7543.2001 PMID: 11705930; PubMed Central PMCID: PMC98844.

41. Carpenter AE, Jones TR, Lamprecht MR, Clarke C, Kang IH, Friman O, et al. CellProfiler: image analysis software for identifying and quantifying cell phenotypes. Genome Biol. 2006; 7(10):R100. Epub 2006/11/02. https://doi.org/10.1186/gb-2006-7-10-r100 PMID: 17076895; PubMed Central PMCID: PMC1794559.

42. Schindelin J, Arganda-Carreras I, Frise E, Kaynig V, Longair M, Pietzsch T, et al. Fiji: an open-source platform for biological-image analysis. Nat Methods. 2012; 9(7):676–82. Epub 2012/06/30. https://doi.org/10.1038/nmeth.2019 PMID: 22743772; PubMed Central PMCID: PMC3855844.